INTERNATIONAL JOURNAL FOR NUMERICAL METHODS IN ENGINEERING
Int. J. Numer. Meth. Engng 2009; **79**:340–374
Published online 2 February 2009 in Wiley InterScience (www.interscience.wiley.com). DOI: 10.1002/nme.2562

High-order doubly asymptotic open boundaries for scalar wave equation

Suriyon Prempramote[1], Chongmin Song[1,*,†], Francis Tin-Loi[1] and Gao Lin[2]

[1]*School of Civil and Environmental Engineering, University of New South Wales, Sydney, NSW 2052, Australia*
[2]*School of Civil and Hydraulic Engineering, Dalian University of Technology, Dalian 116024, China*

SUMMARY

High-order doubly asymptotic open boundaries are developed for transient analyses of scalar waves propagating in a semi-infinite layer with a constant depth and a circular cavity in a full-plane. The open boundaries are derived in the frequency domain as doubly asymptotic continued fraction solutions of the dynamic stiffness of the unbounded domains. Each term of the continued fraction is a linear function of the excitation frequency. The constants of the continued fraction solutions are determined recursively. The continued fraction solution is expressed in the time domain as ordinary differential equations, which can be solved by standard time-stepping schemes. No parameters other than the orders of the low- and high-frequency expansions need to be selected by users. Numerical experiments demonstrate that evanescent waves and long-time (low-frequency) responses are simulated accurately. In comparison with singly asymptotic open boundaries, significant gain in accuracy is achieved at no additional computational cost. Copyright © 2009 John Wiley & Sons, Ltd.

Received 13 July 2008; Revised 23 December 2008; Accepted 24 December 2008

KEY WORDS: open boundary; doubly asymptotic; continued fraction; wave propagation; absorbing boundary; transmitting boundary

1. INTRODUCTION

When wave propagation problems are modeled, it is often necessary to introduce an artificial boundary around the region of interest so that the size of computational domain is limited to allow the application of well-established numerical methods such as the finite element method. The region exterior to the artificial boundary is regarded as an unbounded domain. A boundary condition mimicking the unbounded domain has to be enforced on the artificial boundary to prevent

*Correspondence to: Chongmin Song, School of Civil and Environmental Engineering, University of New South Wales, Sydney, NSW 2052, Australia.
†E-mail: c.song@unsw.edu.au

Contract/grant sponsor: The Dalian University of Technology
Contract/grant sponsor: The Natural Science Foundation of China; contract/grant number: 90510018

fictitious reflections that pollute the solution. A direct time-domain formulation of the boundary condition is required when non-linearities occur in the region of interest. Such a boundary condition is known by various names such as absorbing, non-reflecting, open, radiation, transmitting and transparent boundary conditions. In this paper, only the term 'open boundary' is employed to refer to the artificial boundary with a boundary condition mimicking the unbounded domain. Extensive literature on various open boundaries exists. Excellent literature reviews are available in papers [1–6] and books [7–10].

In theory, an exact open boundary is global in space and time, i.e. the present response at a point on the boundary is a function of the response history at all boundary points up to the present time. When a rigorous method (for example, the boundary element method [11, 12], the thin-layer method [13] or the scaled boundary finite element method [10, 14]) is employed to construct an open boundary, the formulation is global. The convolution integral and storage of the response history are computationally expensive for large-scale problems and long-time calculations.

Time realization techniques have been proposed to construct temporally local open boundaries from the dynamic stiffness matrices obtained at discrete frequencies from analytical solution or by a rigorous method. In References [15–17], a Padé approximation of the dynamic stiffness matrix is constructed by using a curve fitting technique based on the least-squares method. A temporally local open boundary is formulated after expressing the Padé approximation as unit fractions. In Reference [18], the Padé approximation is expressed as a continued fraction leading to a mixed-variable method. In Reference [19], system theory is applied to construct a temporally local open boundary from the unit-impulse response obtained from the scaled boundary finite element method.

Moreover, a large number of approximate open boundary conditions have been developed. Well-known examples include the viscous boundary [20], the superposition boundary [21], the paraxial boundary [22] and the extrapolation boundary [23]. Generally speaking, they are spatially and temporally local, i.e. the response at a point is coupled with the response at a few adjacent points during a few previous time steps only. These local open boundaries are simple and computationally efficient by themselves, but have to be applied to an artificial boundary sufficiently away from the region of interest in order to obtain results of acceptable accuracy. This increases the total computational effort.

To increase the accuracy and efficiency of simple open boundaries, high-order local open boundaries have been proposed. This type of open boundary has the potential of leading to accurate results as the order of approximation increases. At the same time, it is computationally efficient owing to its local formulation. Examples of early developments include the paraxial boundary [22], the Bayliss, Gunzburger and Turkel (BGT) boundary [24] and the multi-direction boundary [25]. However, the order of derivative in these formulations increases with the order of the open boundary. Beyond the second order, the implementation in a finite element computer program becomes complex and instability may occur [8].

Researchers in several fields have shown their strong interest in developing open boundaries of arbitrarily high order (see, e.g. [26–32]). Literature reviews are available, e.g. in References [4, 6]. Most of the open boundaries are, however, limited to straight, circular and spherical boundaries. Special corner conditions have to be devised for rectangular boundaries. Krenk [30] showed that several of well-established open boundaries can be formulated as a rational function approximation (Padé or continued fraction expansion) of the plane wave representation for scalar waves.

All the above high-order open boundaries were constructed to absorb propagating waves radiating energy. As they are singly asymptotic at the high-frequency limit, these high-order open boundaries

DOI: 10.1002/nme

are appropriate for radiative fields, i.e. virtually all of the field energy is propagating out to infinity [33]. In some classes of applications, a part of the total energy may be trapped near the region of interest and may not propagate to infinity. The best-known example is probably the evanescent waves occurring in a semi-infinite layer with a constant depth (also known as a waveguide). It is explained in Reference [34] that inclusion of evanescent modes improves the accuracy of the long-time behavior of a high-order open boundary. Another example is the class of problems where the dimensionless frequency $a_0 = \omega r_0/c$ (ω is the smallest excitation frequency of interest, r_0 is a characteristic length of the region of interest, c is the wave velocity) is very low (statics can be regarded as the limiting case $a_0 \to 0$). These wave fields are largely non-radiative. To achieve reasonably accurate results at low frequencies, i.e. over long time, the order of an open boundary has to be very high, thereby leading to large computational cost. In most of the publications on high-order open boundaries, the numerical results are shown for only the first few periods, and long-time responses are rarely reported.

From an application point of view, it is highly desirable to develop a temporally local open boundary that is capable of accurately mimicking an unbounded domain over the entire frequency range (i.e. from zero to infinity). One advance toward this objective is the introduction of the doubly asymptotic boundaries [33, 35–38]. This formulation is spatially global as the dynamic stiffness is exact not only at the high-frequency limit but also at statics. To the knowledge of the authors, the highest order reported is three [39].

Recently, a new approach to construct temporally local open boundaries of arbitrarily high order has been proposed in Reference [40]. It is applicable to both scalar and vector waves. The geometry of the boundary of the unbounded domain can be arbitrary as long as the scaling requirement (there exists a zone from where the whole boundary is visible) is satisfied. Anisotropic unbounded media are handled without additional computation cost. Different from most of existing approaches, it seeks a continued fraction solution for the equation of the dynamic stiffness matrix of an unbounded domain obtained in the scaled boundary finite element method [14]. Each term of the continued fraction is a linear function of the excitation frequency ω. The constant matrices in the continued fraction are determined recursively by satisfying the scaled boundary finite element equation at the high-frequency limit. No explicit solution of the dynamic stiffness matrix at discrete frequencies is required. By using the continued fraction solution, the force–displacement relationship of the unbounded domain is formulated as a temporally local open boundary condition in the time domain. However, like other high-order open boundaries, this open boundary is inappropriate to model evanescent waves, and the convergence rate at low frequencies is much slower than that at high frequencies.

In this paper, a technique for constructing a high-order doubly asymptotic open boundary is proposed by extending the work in Reference [40]. Only scalar waves and unbounded domains with simple geometry, namely a semi-infinite layer with a constant depth (a waveguide) and a circular cavity in a full-plane, are considered. Nevertheless, the open boundaries for these cases can be applied directly to solve practical problems by introducing straight or circular artificial boundaries [17, 26, 27, 29, 34]. The investigations into the simple cases also provide insights into the basic numerical phenomena involved in high-order open boundaries such as the failure in representing evanescent waves and the relative poor performance at low frequencies. Furthermore, a novel approach to develop accuracy and efficient open boundaries is proposed. Further research on modeling problems with more complicated geometry and vector waves is in progress.

This paper is organized as follows. In Section 2, the scalar wave equation is decomposed into a series of one-dimensional wave equations by applying the method of separation of variables.

DOI: 10.1002/nme

After the dynamic stiffness coefficient of a one-dimensional wave problem is introduced, an equation of the dynamic stiffness coefficient is derived. In Section 3, a doubly asymptotic continued fraction solution for the dynamic stiffness coefficient is determined recursively at the high- and low-frequency limits. The link between the singly asymptotic high-frequency solution for the semi-infinite layer and several other high-order open boundaries based on Padé (or continued fraction) expansions is identified. In Section 4, an equation of motion of an unbounded domain is formulated on the boundary by using the doubly asymptotic continued fraction solution of dynamic stiffness. It leads to a temporally local open boundary expressed in time-independent static stiffness and damping matrices. Well-established time-stepping schemes in structural dynamics are directly applicable. In Section 5, the high performance of the proposed high-order doubly asymptotic open boundaries is demonstrated with numerical examples. In Section 6, conclusions are presented.

2. DYNAMIC STIFFNESS OF UNBOUNDED DOMAINS

The linear homogeneous scalar wave equation is expressed as

$$\nabla^2 u = \frac{1}{c^2}\ddot{u} \tag{1}$$

where $u = u(x, y, z, t)$ denotes the wave field, ∇^2 the Laplace operator and c the given wave speed. In this paper, the arguments of functions are omitted for simplicity in the nomenclature. The initial conditions for an unbounded domain initially at rest are expressed as

$$u = \dot{u} = 0 \quad \text{at } t = 0 \tag{2}$$

The geometries and boundary conditions of the semi-infinite layer and the circular cavity are given in Sections 2.1 and 2.2, respectively. By employing the method of separation of variables, Equation (1) can be transformed to a series of one-dimensional wave equations. From a one-dimensional wave equation and the definition of a dynamic stiffness coefficient, an equation of the dynamic stiffness coefficient is then derived.

2.1. Semi-infinite layer with constant depth

A semi-infinite layer with a constant depth h is shown in Figure 1. For convenience, the x-axis of the coordinate system is chosen at the lower boundary of the layer. The formulation of the proposed open boundaries is based on the dynamic stiffness representing the property of the semi-infinite layer. It is independent of the coordinate system. The open boundaries are applicable to semi-infinite layers of any orientation. It is assumed that a distributed traction $\tau_0(t)$ is applied to the vertical boundary Γ_V (at $x = x_0$). The homogeneous boundary conditions prescribed on the

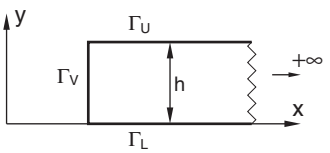

Figure 1. Semi-infinite layer with constant depth.

DOI: 10.1002/nme

parallel upper boundary Γ_U and lower boundary Γ_L are satisfied in the method of separation of variables by eigenfunctions. For example, when the upper boundary Γ_U is free (i.e. $u_{,y}(y=h)=0$) and the lower boundary Γ_L is fixed (i.e. $u(y=0)=0$) the eigenfunctions are $\sin(\lambda_i y/h)$ where the eigenvalues are equal to $\lambda_i=(2i+1)\pi/2$ for $i=0,1,\ldots$. Note that as the eigenvalue λ_i increases, the eigenfunction varies more rapidly along the vertical boundary.

For a mode with a modal eigenvalue λ, the one-dimensional wave equation is expressed as

$$\frac{\partial^2 \tilde{u}}{\partial x^2} - \left(\frac{\lambda}{h}\right)^2 \tilde{u} = \frac{1}{c^2}\ddot{\tilde{u}} \tag{3}$$

where $\tilde{u}=\tilde{u}(x,t)$ is the modal displacement. The modal traction is denoted as $\tilde{\tau}_0(t)$ at $x=x_0$. Once the solution of Equation (3) satisfying both the boundary condition at $x=x_0$ and the radiation condition at $x\to+\infty$ is known, the solution for the wave propagation in the semi-infinite layer can be obtained by modal superposition. Hereafter, only the modal equation in Equation (3) is addressed, and the word 'modal' is omitted for the sake of simplicity except where confusion may arise.

By assuming the time-harmonic behavior $\tilde{u}=\widetilde{U}(\omega,x)\mathrm{e}^{+\mathrm{i}\omega t}$ and $\tilde{\tau}_0(t)=\widetilde{R}(\omega,x)\mathrm{e}^{+\mathrm{i}\omega t}$ (ω is the excitation frequency), Equation (3) is rewritten in the frequency domain as

$$\frac{\mathrm{d}^2\widetilde{U}}{\mathrm{d}x^2} + \frac{1}{h^2}(a_0^2-\lambda^2)\widetilde{U} = 0 \tag{4}$$

where $\widetilde{U}=\widetilde{U}(\omega,x)$ is the displacement amplitude and a_0 is a dimensionless frequency

$$a_0 = \frac{\omega h}{c} \tag{5}$$

2.1.1. Analytical solution. The solution of Equation (4) satisfying the radiation condition for the semi-infinite layer extending to $x\to+\infty$ (Figure 1) is

$$\widetilde{U} = C\mathrm{e}^{-\sqrt{\lambda^2-a_0^2}x/h} \tag{6}$$

with the integration constant C. A cut-off frequency exists in Equation (6) at the dimensionless frequency $a_0=\lambda$. Below the cut-off frequency, i.e. $a_0<\lambda$, the displacement decays exponentially. No propagating waves exist, in other words, evanescent waves are present. Above the cut-off frequency, i.e. $a_0>\lambda$, Equation (6) describes a wave propagating with a frequency-dependent phase velocity.

For the semi-infinite layer extending to the right-hand side, the force amplitude $\widetilde{R}=\widetilde{R}(\omega,x)$ on a vertical boundary at arbitrary x is expressed as

$$\widetilde{R} = -h\frac{\mathrm{d}\widetilde{U}}{\mathrm{d}x} \tag{7}$$

Substituting Equation (6) into Equation (7) results in

$$\widetilde{R} = -h\frac{\mathrm{d}\widetilde{U}}{\mathrm{d}x} = C\sqrt{\lambda^2-a_0^2}\,\mathrm{e}^{-\sqrt{\lambda^2-a_0^2}x/h} \tag{8}$$

DOI: 10.1002/nme

The open boundary condition is represented as a force–displacement relationship. In the frequency domain, this relationship is defined by the dynamic stiffness coefficient $S=S(\omega,x)$ at a vertical line with a constant x-coordinate

$$\widetilde{R}=S\widetilde{U} \tag{9}$$

It is analogous to the DtN operator [41]. The solution for the dynamic stiffness coefficient can be obtained from its definition in Equation (9) with the substitution of Equations (6) and (8)

$$S(a_0)=\sqrt{\lambda^2-a_0^2} \tag{10}$$

Note that the dynamic stiffness coefficient $S(a_0)$ is only a function of the dimensionless frequency a_0 and is independent of the value of the x coordinate (Equation (5)). Below the cut-off frequency, i.e. $a_0<\lambda$, $S(a_0)$ is a real number whereas the imaginary part representing radiation damping vanishes. At the cut-off frequency $a_0=\lambda$, $S(a_0)$ is equal to zero representing the resonance of the semi-infinite layer. Above the cut-off frequency, i.e. $a_0>\lambda$, $S(a_0)$ is pure imaginary. Equation (10) normalized by the modal eigenvalue λ is the square-root operator widely used in constructing open boundaries

$$\frac{S(a_0)}{\lambda}=\sqrt{1-\left(\frac{a_0}{\lambda}\right)^2} \tag{11}$$

To obtain a reference solution to validate numerical results in the time domain, the response to a unit impulse of traction $\tilde{\tau}_{0\mathrm{I}}(t)=\delta(t)$ ($\delta(t)$ represents the Dirac-delta function) applied at $x=x_0$ is evaluated. The amplitude of the displacement response $\widetilde{U}_{\mathrm{I}}$ is determined from Equations (10) and (9) with the Fourier transform of the unit impulse $\widetilde{R}_{0\mathrm{I}}=1$

$$\widetilde{U}_{\mathrm{I}}=\frac{1}{\sqrt{\lambda^2-a_0^2}} \tag{12}$$

The unit-impulse response $\tilde{u}_{\mathrm{I}}(t)$ is equal to the inverse Fourier transform of $\widetilde{U}_{\mathrm{I}}$ (Equation (12))

$$\tilde{u}_{\mathrm{I}}(t)=\frac{c}{h}J_0\left(\lambda\frac{ct}{h}\right)H(t) \tag{13}$$

where J_0 is the zero order first kind Bessel function, $H(t)$ is the Heaviside-step function ($H(t<0)=0$, $H(t\geqslant 0)=1$), and $\bar{t}=ct/h$ represents the dimensionless time. At large time ($\bar{t}\gg 1$), the asymptotic solution of the unit-impulse response is expressed as

$$\tilde{u}_{\mathrm{I}}(t)\to\sqrt{\frac{2h}{\pi\lambda ct}}\cos\left(\lambda\frac{ct}{h}-\frac{\pi}{4}\right) \tag{14}$$

It oscillates at a period of $T=2\pi h/(\lambda c)$. This period corresponds to the dimensionless cut-off frequency $a_0=\lambda$ where the dynamic stiffness coefficient is equal to zero. The unit-impulse response exhibits a long-lasting oscillation with a very slow decay rate of $\sqrt{T/t}$ (see Figure 14 in Section 5.1).

The displacement response to a prescribed traction $\tilde{\tau}_0(t)$ is expressed as a convolution integral

$$\tilde{u}(t)=\frac{c}{h}\int_0^t J_0\left(\lambda\frac{c(t-\tau)}{h}\right)\tilde{\tau}_0(\tau)\,\mathrm{d}\tau \tag{15}$$

DOI: 10.1002/nme

2.1.2. Equation of dynamic stiffness coefficient. An equation of the dynamic stiffness coefficient is derived from the wave equation and the definition of the dynamic stiffness coefficient. Eliminating the force amplitude $\widetilde{R}$ from Equations (7) and (9) leads to

$$h\frac{\mathrm{d}\widetilde{U}}{\mathrm{d}x}=-S\widetilde{U} \tag{16}$$

Differentiating Equation (16) with respect to x and multiplying the result by h yield

$$h^2\frac{\mathrm{d}^2\widetilde{U}}{\mathrm{d}x^2}=-Sh\frac{\mathrm{d}\widetilde{U}}{\mathrm{d}x}-h\frac{\mathrm{d}S}{\mathrm{d}x}\widetilde{U}=\left(S^2-h\frac{\mathrm{d}S}{\mathrm{d}x}\right)\widetilde{U} \tag{17}$$

Substituting Equation (17) into Equation (4) multiplied by h^2 results, for an arbitrary $\widetilde{U}$, in

$$S^2-\frac{\mathrm{d}S}{\mathrm{d}x}+a_0^2-\lambda^2=0 \tag{18}$$

As both a_0 (Equation (5)) and the eigenvalue λ are independent of x, the dynamic stiffness coefficient is a function of a_0 only, i.e. $\mathrm{d}S/\mathrm{d}x=0$. Equation (18) is, therefore, rewritten as

$$(S(a_0))^2+a_0^2-\lambda^2=0 \tag{19}$$

Its positive solution is given in Equation (10).

2.2. Circular cavity embedded in full-plane

The scalar wave propagation in a full-plane with a circular cavity of radius r_0 (Figure 2) is addressed. A surface traction $\tau_0(t)$ is applied on the boundary Γ. Applying the method of separation of variables to the scalar wave equation in polar coordinates r, θ leads to a series of wave equations in the radial direction

$$r^2\frac{\mathrm{d}^2\widetilde{u}}{\mathrm{d}r^2}+r\frac{\mathrm{d}\widetilde{u}}{\mathrm{d}r}-\lambda^2\widetilde{u}=\left(\frac{r}{c}\right)^2\ddot{\widetilde{u}} \tag{20}$$

where $\tilde{u}=\tilde{u}(r,t)$ is the modal displacement, λ is the modal eigenvalue. The modal traction is denoted as $\tilde{\tau}_0(t)$ at $r=r_0$. In the frequency domain ($\widetilde{U}=\widetilde{U}(\omega,r)$ is the displacement amplitude), Equation (20) is expressed as a Bessel equation of order λ

$$r^2\frac{\mathrm{d}^2\widetilde{U}}{\mathrm{d}r^2}+r\frac{\mathrm{d}\widetilde{U}}{\mathrm{d}r}+\left(\left(\frac{\omega r}{c}\right)^2-\lambda^2\right)\widetilde{U}=0 \tag{21}$$

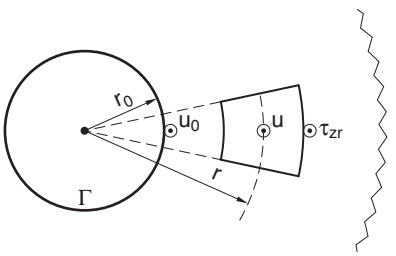

Figure 2. Circular cavity embedded in full-plane.

DOI: 10.1002/nme

2.2.1. Analytical solution. The solution of Equation (21) satisfying the radiation condition is the second-kind Hankel function of order λ

$$\widetilde{U} = C H_{\lambda}^{(2)}(a) \tag{22}$$

with the dimensionless variable

$$a = a(\omega, r) = \frac{\omega r}{c} \tag{23}$$

and the integration constant C. The force amplitude $\widetilde{R} = \widetilde{R}(\omega, r)$ on a circle of radius r is expressed as

$$\widetilde{R} = -r \frac{\mathrm{d}\widetilde{U}}{\mathrm{d}r} \tag{24}$$

Substituting Equation (22) into Equation (24) results in

$$\widetilde{R} = -Cr \frac{\mathrm{d}H_{\lambda}^{(2)}(a)}{\mathrm{d}r} \tag{25}$$

The dynamic stiffness coefficient $S = S(\omega, r)$ relating the force amplitude to the displacement amplitude on a circle of radius r is defined as

$$\widetilde{R} = S\widetilde{U} \tag{26}$$

It is obtained from Equations (26), (25) and (22) and expressed as

$$S(a) = -\frac{a}{H_{\lambda}^{(2)}(a)} \frac{\mathrm{d}H_{\lambda}^{(2)}(a)}{\mathrm{d}a} = \lambda - \frac{H_{\lambda-1}^{(2)}(a)}{H_{\lambda}^{(2)}(a)} \tag{27}$$

Note that the only independent variable is the dimensionless variable a. The dynamic stiffness coefficient on the boundary Γ of the circular cavity is determined by evaluating $S(a)$ at $r = r_0$.

2.2.2. Equation of dynamic stiffness coefficient. To derive an equation of the dynamic stiffness coefficient $S = S(\omega, r)$, the force amplitude $\widetilde{R}$ is eliminated from Equations (24) and (26). This leads to

$$r \frac{\mathrm{d}\widetilde{U}}{\mathrm{d}r} = -S\widetilde{U} \tag{28}$$

Differentiating Equation (28) and multiplying the resulting expression by r result in

$$r^2 \frac{\mathrm{d}^2\widetilde{U}}{\mathrm{d}r^2} + r \frac{\mathrm{d}\widetilde{U}}{\mathrm{d}r} = -Sr \frac{\mathrm{d}\widetilde{U}}{\mathrm{d}r} - r \frac{\mathrm{d}S}{\mathrm{d}r}\widetilde{U} = \left(S^2 - r \frac{\mathrm{d}S}{\mathrm{d}r}\right)\widetilde{U} \tag{29}$$

Substituting Equation (29) into Equation (21) and then eliminating $\widetilde{U}$ lead to an equation of the dynamic stiffness coefficient

$$S^2 - r \frac{\mathrm{d}S}{\mathrm{d}r} + \left(\frac{\omega r}{c}\right)^2 - \lambda^2 = 0 \tag{30}$$

DOI: 10.1002/nme

Changing the independent variable from r to the dimensionless variable a (Equation (23)) yields

$$(S(a))^2 - a\frac{\mathrm{d}S(a)}{\mathrm{d}a} + a^2 - \lambda^2 = 0 \tag{31}$$

The number of independent variables is now reduced from two (ω and r) to one (a). To construct an open boundary, it is sufficient to consider the dynamic stiffness coefficient on the boundary Γ. Equation (31) is thus expressed at $r = r_0$ as

$$(S(a_0))^2 - a_0\frac{\mathrm{d}S(a_0)}{\mathrm{d}a_0} + a_0^2 - \lambda^2 = 0 \tag{32}$$

with the dimensionless frequency

$$a_0 = \frac{\omega r_0}{c} \tag{33}$$

2.3. Comparison between dynamic stiffness coefficients of semi-infinite layer and circular cavity

The dynamic stiffness coefficients of the semi-infinite layer and the circular cavity are normalized with the eigenvalue λ to examine their interrelationship. Equation (19) is thus rewritten as

$$\left(\frac{S(a_0)}{\lambda}\right)^2 + \left(\frac{a_0}{\lambda}\right)^2 - 1 = 0 \tag{34}$$

and Equation (32) as

$$\left(\frac{S(a_0)}{\lambda}\right)^2 - \frac{1}{\lambda}\left(\frac{a_0}{\lambda}\right)\frac{\mathrm{d}}{\mathrm{d}(a_0/\lambda)}\left(\frac{S(a_0)}{\lambda}\right) + \left(\frac{a_0}{\lambda}\right)^2 - 1 = 0 \tag{35}$$

Equation (35) can be regarded as an ordinary differential equation of $S(a_0)/\lambda$ with the independent variable a_0/λ. The contribution of its second term decreases as λ increases. At the limit of $\lambda \to \infty$, the ordinary differential equation in Equation (35) degenerates to the algebraic equation in Equation (34). Therefore, the dynamic stiffness coefficient of a mode of the circular cavity tends to that of a mode of the semi-infinite layer with the same eigenvalue λ (Equation (11)). This is illustrated in Figure 3 by comparing the normalized dynamic stiffness coefficient $S(a_0)/\lambda$ of

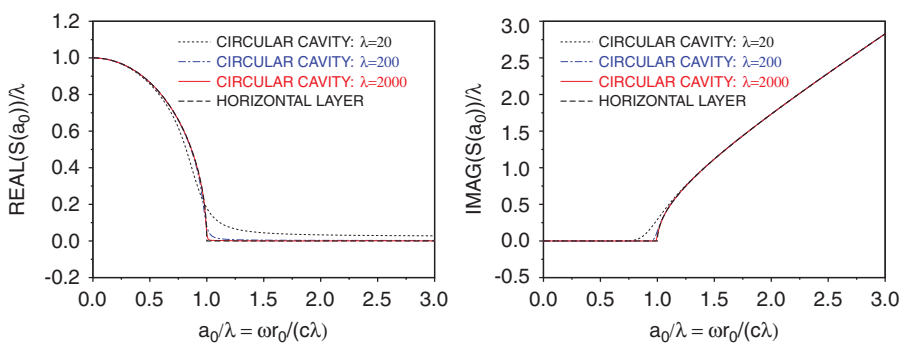

Figure 3. Comparison of dynamic stiffness coefficients of semi-infinite layer and circular cavity.

DOI: 10.1002/nme

the cylindrical cavity (Equation (27) with $a=a_0$ on boundary) for modes $\lambda=20$, 200 and 2000 with the dynamic stiffness coefficient of the semi-infinite layer (Equation (11)). As λ increases, the dynamic stiffness coefficient of the cylindrical cavity approaches that of the semi-infinite layer ($a_0=\omega h/c$). At $\lambda=2000$, the two dynamic stiffness coefficients become nearly indistinguishable.

3. DOUBLY ASYMPTOTIC CONTINUED FRACTION SOLUTION FOR DYNAMIC STIFFNESS

A continued fraction solution of the dynamic stiffness coefficient is obtained recursively in Reference [40] as a singly asymptotic solution at the high-frequency limit ($\omega\to+\infty$). It is shown for the circular cavity problem that the solution converges rapidly to the exact solution when the order of continued fraction increases and the dimensionless frequency is larger than the modal eigenvalue λ. At lower frequency range, the error increases significantly and the convergence is much slower. As it will be demonstrated in Section 5.1, the high-frequency continued fraction solution does not converge at all for the semi-infinite layer problem when the frequency is below the cut-off frequency.

A doubly asymptotic continued fraction solution is developed to improve the behavior of the singly asymptotic solution. After the high-frequency continued fraction solution is determined as in Reference [40], the differential equation of the residual term is solved again as a continued fraction, but the constants are determined at the low-frequency limit ($\omega\to 0$).

Equation (19) for the semi-infinite layer is an algebraic equation, and Equation (32) for the circular cavity is an ordinary differential equation. They are addressed in Sections 3.1 and 3.2, respectively.

3.1. Semi-infinite layer with constant depth

3.1.1. High-frequency continued fraction. The construction of the high-frequency continued fraction solution for Equation (19) follows the procedure in Reference [40]. In this particular case, an order M_{H} continued fraction solution is expressed as

$$S(a_0)=(\mathrm{i}a_0)C_\infty-\cfrac{\lambda^2}{(\mathrm{i}a_0)Y_1^{(1)}-\cfrac{\lambda^2}{(\mathrm{i}a_0)Y_1^{(2)}-\cfrac{\lambda^2}{\cdots-\cfrac{\lambda^2}{(\mathrm{i}a_0)Y_1^{(M_{\mathrm{H}})}-\cfrac{\lambda^2}{Y^{(M_{\mathrm{H}}+1)}(a_0)}}}}} \tag{36}$$

where the constants C_∞ and $Y_1^{(i)}$ ($i=1,2,\ldots,M_{\mathrm{H}}$) are determined by satisfying Equation (19) at the high-frequency limit $a_0\to+\infty$. The negative sign in front of each term is selected intentionally so that the open boundary can be easily expressed with symmetric coefficient matrices (see Section (4)). Equation (36) is equivalent to

$$S(a_0)=(\mathrm{i}a_0)C_\infty-\lambda^2(Y^{(1)}(a_0))^{-1} \tag{37a}$$

$$Y^{(i)}(a_0)=(\mathrm{i}a_0)Y_1^{(i)}-\lambda^2(Y^{(i+1)}(a_0))^{-1}\quad(i=1,2,\ldots,M_{\mathrm{H}}) \tag{37b}$$

DOI: 10.1002/nme

where $Y^{(1)}(a_0)$ is of the order $(\mathrm{i}a_0)^{-1}$ as $a_0 \to +\infty$. When a singly asymptotic solution is considered, the residual term $\lambda^2(Y^{(M_H+1)}(a_0))^{-1}$ is neglected.

Substituting Equation (37a) into Equation (19) results in an equation in terms of a power series of $(\mathrm{i}a_0)$

$$(\mathrm{i}a_0)^2(C_\infty^2-1)+\lambda^2(-1-2(\mathrm{i}a_0)C_\infty(Y^{(1)}(a_0))^{-1}+\lambda^2(Y^{(1)}(a_0))^{-2})=0 \tag{38}$$

This equation is satisfied by setting, in descending order, the two terms to zero. The first term is an equation for damping coefficient C_∞. To satisfy the radiation condition, the positive solution is chosen

$$C_\infty = 1 \tag{39}$$

The second term of Equation (38) is an equation of $Y^{(1)}(a_0)$ as C_∞ is known (Equation (39)). To derive a recursive formula for determining the constants of the continued fraction, it is rewritten as the $i=1$ case of

$$\lambda^2-2b_1^{(i)}(\mathrm{i}a_0)Y^{(i)}(a_0)-(Y^{(i)}(a_0))^2=0 \tag{40}$$

with the constant

$$b_1^{(1)}=1 \tag{41}$$

Substituting Equation (37b) into Equation (40) leads to an equation in terms of a power series of $(\mathrm{i}a_0)$

$$-(\mathrm{i}a_0)^2((Y_1^{(i)})^2+2b_1^{(i)}Y_1^{(i)})+\lambda^2(1+2(\mathrm{i}a_0)(Y_1^{(i)}+b_1^{(i)})(Y^{(i+1)}(a_0))^{-1}-\lambda^2(Y^{(i+1)}(a_0))^{-2})=0 \tag{42}$$

Again, this equation is satisfied by setting the two terms to zero. The non-zero solution of the $(\mathrm{i}a_0)^2$ term is equal to

$$Y_1^{(i)}=-2b_1^{(i)} \tag{43}$$

By using the solution of $Y_1^{(i)}$ in Equation (43), the second term of Equation (42) is rearranged as

$$\lambda^2+2b_1^{(i)}(\mathrm{i}a_0)Y^{(i+1)}(a_0)-(Y^{(i+1)}(a_0))^2=0 \tag{44}$$

Introducing the recursive formula for updating the constant

$$b_1^{(i+1)}=-b_1^{(i)} \tag{45}$$

Equation (44) is simply the $(i+1)$ case of Equation (40). From Equations (41) and (45),

$$b_1^{(i)}=(-1)^{i+1} \tag{46}$$

applies. $Y_1^{(i)}$ is obtained explicitly from Equation (43) as

$$Y_1^{(i)}=(-1)^i 2 \tag{47}$$

DOI: 10.1002/nme

The high-frequency continued fraction solution in Equation (36) (or Equation (37)) is constructed from the solutions of the constants C_∞ in Equation (39) and $Y_1^{(i)}$ in Equation (47). For example, Equation (36) is expressed for the order $M_H=2$ high-frequency continued fraction as

$$S(a_0)=(\mathrm{i}a_0)-\cfrac{\lambda^2}{-2(\mathrm{i}a_0)-\cfrac{\lambda^2}{2(\mathrm{i}a_0)-\cfrac{\lambda^2}{Y^{(3)}(a_0)}}} \tag{48}$$

3.1.2. Link with other open boundaries for plane waves. The singly asymptotic continued fraction solution in Equation (36) is expressed by using Equations (39) and (47) as

$$\frac{S(a_0)}{(\mathrm{i}a_0)}=1-\cfrac{(\lambda/(\mathrm{i}a_0))^2}{-2-\cfrac{(\lambda/(\mathrm{i}a_0))^2}{2-\cfrac{(\lambda/(\mathrm{i}a_0))^2}{-2-\cdots}}}=1+\cfrac{(\lambda/(\mathrm{i}a_0))^2}{2+\cfrac{(\lambda/(\mathrm{i}a_0))^2}{2+\cfrac{(\lambda/(\mathrm{i}a_0))^2}{2+\cdots}}}=1-\cfrac{(\lambda/a_0)^2}{2-\cfrac{(\lambda/a_0)^2}{2-\cfrac{(\lambda/a_0)^2}{2-\cdots}}} \tag{49}$$

Several open boundaries have been constructed based on the continued fractions of the function $\sqrt{1+x}$, where x may represent the wave number, pseudo-differential operator or the angle of incidence of a plane wave depending on the particular formulation. For example, the third approximation expressed in Equation (1.13) of Reference [42] is based on the continued fraction

$$\sqrt{1+x}=1+\cfrac{x}{2+\cfrac{x}{2}} \tag{50}$$

When $x=(\lambda/\mathrm{i}a_0)^2=-(\lambda/a_0)^2$ is assumed, Equation (50) is equivalent to the second-order singly asymptotic continued fraction in Equation (49).

It has been shown in Reference [30] that, when all the angles of ideal transmission are selected as 0, the multi-directional open boundary proposed by Higdon [43] corresponds to the continued fraction of $\cos\theta=\sqrt{1-\sin^2\theta}$ (Equation (15), [30])

$$\cos\theta=1-\cfrac{\sin^2\theta}{2-\cfrac{\sin^2\theta}{2-\cfrac{\sin^2\theta}{2-\cdots}}} \tag{51}$$

where θ is the angle of incidence (the angle between the direction of propagation of a plane wave and the outward normal of the boundary). Equation (51) is equivalent to Equation (50) for the same order of continued fraction when $x=-\sin^2\theta$ is assumed. By comparing Equation (49) with Equation (51), it can be identified that the two equations are identical when setting

$$\sin\theta=\lambda/a_0 \tag{52}$$

Equation (52) relates the dimensionless frequency a_0 to the angle of incidence θ.

As $\sin\theta$ is bounded between 0 and 1, the performance of open boundaries based on this continued fraction is controlled for $a_0\geqslant\lambda$, i.e. above the cut-off frequency, only. Their accuracy below the

DOI: 10.1002/nme

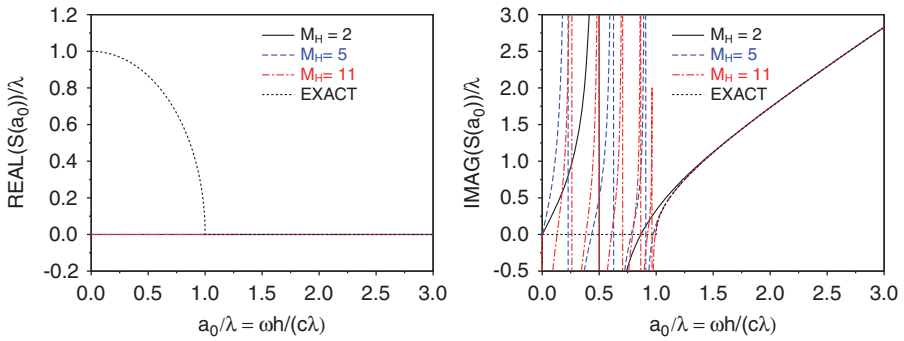

Figure 4. High-frequency continued fraction solution for dynamic stiffness coefficient of semi-infinite layer.

cut-off frequency ($a_0<\lambda$), i.e. for the evanescent waves, is not guaranteed. This is illustrated in Figure 4 by comparing the continued fraction solution with the exact solution (Equation (10)). The dynamic stiffness coefficient and the dimensionless frequency are normalized as expressed in Equation (11). When the frequency is slightly above the cut-off frequency ($a_0/\lambda>1.25$), the order $M_{\mathrm{H}}=2$ continued fraction solution is already very accurate. However, the error below the cut-off frequency is very large. The imaginary part exhibits a discontinuous point. The real part of the continued fraction solution is always equal to zero independent of the order as expected from Equation (48). As the order of the continued fraction increases to $M_{\mathrm{H}}=5$ and $M_{\mathrm{H}}=11$, the accuracy of the results at frequencies immediately above the cut-off frequency improves. The result of $M_{\mathrm{H}}=11$ is indistinguishable from the exact solution above the cut-off frequency. Below the cut-off frequency, the number of discontinuous points in the imaginary part increases and the accuracy does not improve. The error at the low-frequency range affects the accuracy of late-time response in the time domain as illustrated numerically in Section 5.1.

A reflection coefficient based on the angle of incidence of propagating plane waves is often derived in the literature to evaluate the performance of an open boundary. It is meaningful for only $0\leqslant\sin\theta\leqslant1$, i.e. the frequency range $a_0\geqslant\lambda$. As the order increases, the reflection coefficient becomes smaller but the accuracy below the cut-off frequency does not necessarily improve. This is consistent with the statement in Reference [34] that: 'a comparison of boundary conditions based solely on the magnitude of reflection coefficients for propagating modes is a poor predictor of actual performance, particularly as the order is increased'.

3.1.3. Doubly asymptotic continued fraction. The procedure in Section 3.1.1 leads to not only a high-frequency continued fraction solution for the dynamic stiffness coefficient but also an equation of the residual term $Y^{(M_{\mathrm{H}}+1)}(a_0)$, i.e. the $i=M_{\mathrm{H}}+1$ case of Equation (40) with the constant $b_1^{(M_{\mathrm{H}}+1)}$ given in Equation (46). To determine a solution that is valid over the whole frequency range, a low-frequency continued fraction solution for the residual term $Y^{(M_{\mathrm{H}}+1)}(a_0)$ is sought.

Denoting the residual term as

$$Y_{\mathrm{L}}(a_0)=Y^{(M_{\mathrm{H}}+1)}(a_0) \tag{53}$$

DOI: 10.1002/nme

the $i = M_H + 1$ case of Equation (40) is expressed as

$$\lambda^2 - 2b_L(\mathrm{i}a_0)Y_L(a_0) - (Y_L(a_0))^2 = 0 \tag{54}$$

with the constant

$$b_L = b_1^{(M_H+1)} = (-1)^{M_H} \tag{55}$$

given in Equation (46). The continued fraction solution for $Y_L(a_0)$ at the low-frequency limit is written as

$$Y_L(a_0) = Y_{L0}^{(0)} + (\mathrm{i}a_0)Y_{L1}^{(0)} - \cfrac{(\mathrm{i}a_0)^2}{Y_{L0}^{(1)} - \cfrac{(\mathrm{i}a_0)^2}{Y_{L0}^{(2)} - \cfrac{(\mathrm{i}a_0)^2}{\cdots - \cfrac{(\mathrm{i}a_0)^2}{Y_{L0}^{(M_L)}}}}} \tag{56}$$

It is equivalent to

$$Y_L(a_0) = Y_{L0}^{(0)} + (\mathrm{i}a_0)Y_{L1}^{(0)} - (\mathrm{i}a_0)^2 (Y_L^{(1)}(a_0))^{-1} \tag{57a}$$

$$Y_L^{(i)}(a_0) = Y_{L0}^{(i)} - (\mathrm{i}a_0)^2 (Y_L^{(i+1)}(a_0))^{-1} \quad (i = 1, 2, \ldots, M_L) \tag{57b}$$

where the constant term in Equation (57b) is omitted as its solution is equal to zero. For an M_L order continued fraction, the residual $(\mathrm{i}a_0)^2 / Y_L^{(i+1)}(a_0)$ is neglected. The constants $Y_{L0}^{(i)}$ $(i = 1, 2, \ldots, M_L)$ and $Y_{L1}^{(0)}$ are determined by satisfying Equation (54) at the low-frequency limit $(a_0 \to 0)$.

Substituting Equation (57a) into Equation (54) leads to an equation in terms of a power series of $(\mathrm{i}a_0)$

$$\begin{aligned}(\lambda^2 - (Y_{L0}^{(0)})^2) - (\mathrm{i}a_0)(2b_L Y_{L0}^{(0)} + 2Y_{L0}^{(0)} Y_{L1}^{(0)}) + (\mathrm{i}a_0)^2(-2b_L Y_{L1}^{(0)} - (Y_{L1}^{(0)})^2 \\ + 2(Y_{L0}^{(0)} + (\mathrm{i}a_0)(Y_{L1}^{(0)} + b_L))(Y_L^{(1)}(a_0))^{-1} - (\mathrm{i}a_0)^2 (Y_L^{(1)}(a_0))^{-2}) = 0\end{aligned} \tag{58}$$

As the low-frequency solution is being sought, Equation (58) is satisfied by setting the coefficients of the power series to zero in ascending order. Setting the constant term to zero results in

$$\lambda^2 - (Y_{L0}^{(0)})^2 = 0 \tag{59}$$

Out of the two solutions, the one leading to the correct static stiffness $S(a_0 = 0) = \lambda$ should be chosen. Inspecting Equation (36) with $Y^{(M_H+1)}(a_0 = 0) = Y_L(a_0 = 0) = Y_{L0}^{(0)}$ (Equations (53) and (57a)), the solution is

$$Y_{L0}^{(0)} = (-1)^{M_H+1} \lambda \tag{60}$$

Setting the coefficient of the $(\mathrm{i}a_0)$ term in Equation (58) to zero leads to an equation for $Y_{L1}^{(0)}$. Using Equation (55), its solution is expressed as

$$Y_{L1}^{(0)} = -b_L = (-1)^{M_H+1} \tag{61}$$

DOI: 10.1002/nme

Setting the coefficient of the $(\mathrm{i}a_0)^2$ term in Equation (58) to zero yields an equation of $Y_{\mathrm{L}}^{(1)}(a_0)$. After substituting the solutions for $Y_{\mathrm{L}0}^{(0)}$ (Equation (60)) and $Y_{\mathrm{L}1}^{(0)}$ (Equation (61)), the equation is expressed as the $i=1$ case of the following equation:

$$(\mathrm{i}a_0)^2 - 2b_{\mathrm{L}}^{(i)} Y_{\mathrm{L}}^{(i)}(a_0) - (Y_{\mathrm{L}}^{(i)}(a_0))^2 = 0 \tag{62}$$

with the constant (Equation (55))

$$b_{\mathrm{L}}^{(1)} = -b_{\mathrm{L}}\lambda = (-1)^{M_{\mathrm{H}}+1}\lambda \tag{63}$$

A recursive procedure for determining the constants $Y_{\mathrm{L}0}^{(i)}$ in Equation (57b) is established by substituting Equation (57b) into Equation (62). The resulting expression is arranged as

$$-(2b_{\mathrm{L}}^{(i)} Y_{\mathrm{L}0}^{(i)} + (Y_{\mathrm{L}0}^{(i)})^2) + (\mathrm{i}a_0)^2 (1 + 2(b_{\mathrm{L}}^{(i)} + Y_{\mathrm{L}0}^{(i)})(Y_{\mathrm{L}}^{(i+1)}(a_0))^{-1} - (\mathrm{i}a_0)^2 (Y_{\mathrm{L}}^{(i+1)}(a_0))^{-2}) = 0 \tag{64}$$

Setting the term independent of $(\mathrm{i}a_0)$ to zero yields an equation for $Y_{\mathrm{L}0}^{(i)}$. Its non-zero solution is

$$Y_{\mathrm{L}0}^{(i)} = -2b_{\mathrm{L}}^{(i)} \tag{65}$$

Setting the $(\mathrm{i}a_0)^2$ term to zero and using Equation (65) result in the equation of $Y_{\mathrm{L}}^{(i+1)}(a_0)$

$$(\mathrm{i}a_0)^2 + 2b_{\mathrm{L}}^{(i)} Y_{\mathrm{L}}^{(i+1)}(a_0) - (Y_{\mathrm{L}}^{(i+1)}(a_0))^2 = 0 \tag{66}$$

It is simply the $(i+1)$ case of Equation (62) with the constant

$$b_{\mathrm{L}}^{(i+1)} = -b_{\mathrm{L}}^{(i)} \tag{67}$$

Equations (63) and (67) lead to

$$b_{\mathrm{L}}^{(i)} = (-1)^{M_{\mathrm{H}}+i}\lambda, \quad i = 1, 2, \ldots, M_{\mathrm{L}} \tag{68}$$

The constants of the continued fraction are expressed explicitly as

$$Y_{\mathrm{L}0}^{(i)} = (-1)^{M_{\mathrm{H}}+i+1} 2\lambda, \quad i = 1, 2, \ldots, M_{\mathrm{L}} \tag{69}$$

As an example, the order $M_{\mathrm{L}}=2$ low-frequency continued fraction for the residual $Y^{(3)}(a_0)$ of the order $M_{\mathrm{H}}=2$ high-frequency continued fraction solution is expressed as

$$Y^{(3)}(a_0) = Y_{\mathrm{L}}(a_0) = -\lambda - (\mathrm{i}a_0) - \cfrac{(\mathrm{i}a_0)^2}{2\lambda - \cfrac{(\mathrm{i}a_0)^2}{-2\lambda}} \tag{70}$$

The doubly asymptotic continued fraction solution is constructed by combining the high-frequency continued fraction solution in Equation (36) (or Equation (37)) with the low-frequency solution in Equation (56) (or Equation (57)) using $Y^{(M_{\mathrm{H}}+1)}(a_0) = Y_{\mathrm{L}}(a_0)$ (Equation (53)). For

DOI: 10.1002/nme

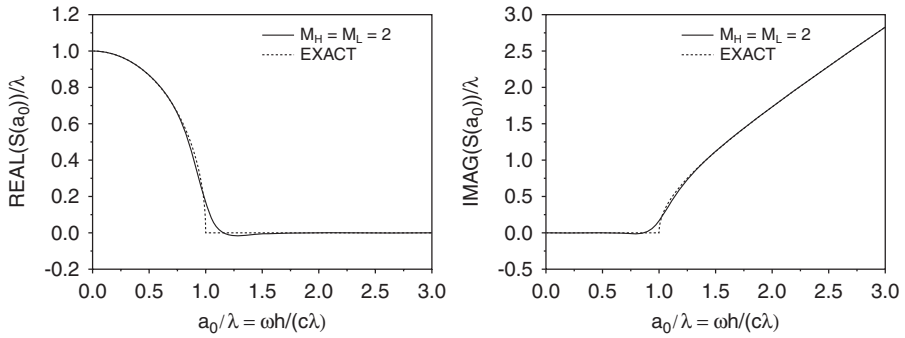

Figure 5. Doubly asymptotic continued fraction solution for dynamic stiffness coefficient of semi-finite layer: $M_{\mathrm{H}}=M_{\mathrm{L}}=2$.

example, the order $M_{\mathrm{H}}=M_{\mathrm{L}}=2$ doubly asymptotic continued fraction solution is obtained from Equations (48) and (70) as

$$S(a_0)=(\mathrm{i}a_0)-\cfrac{\lambda^2}{-2(\mathrm{i}a_0)-\cfrac{\lambda^2}{2(\mathrm{i}a_0)-\cfrac{\lambda^2}{-\lambda-(\mathrm{i}a_0)-\cfrac{(\mathrm{i}a_0)^2}{2\lambda-\cfrac{(\mathrm{i}a_0)^2}{-2\lambda}}}}} \tag{71}$$

The real and imaginary parts of the order $M_{\mathrm{H}}=M_{\mathrm{L}}=2$ doubly asymptotic solution are compared with the exact solution in Figure 5. The present result is very accurate outside of a small range around the cut-off frequency.

Further evaluation of the accuracy of the doubly asymptotic solution is reported in Section 5.1.

3.2. *Circular cavity embedded in full-plane*

3.2.1. High-frequency continued fraction. Like the continued fraction solution in Equation (37) for the semi-infinite layer, the high-frequency continued fraction is expressed as

$$S(a_0)=K_\infty+(\mathrm{i}a_0)C_\infty-(Y^{(1)}(a_0))^{-1} \tag{72a}$$

$$Y^{(i)}(a_0)=Y_0^{(i)}+(\mathrm{i}a_0)Y_1^{(i)}-(Y^{(i+1)}(a_0))^{-1}\quad (i=1,2,\ldots,M_{\mathrm{H}}) \tag{72b}$$

where C_∞ is the damping coefficient, K_∞ the spring coefficient and $(Y^{(1)}(a_0))^{-1}$ the residual term. Substituting Equation (72a) into Equation (31) yields an equation in terms of a power series of $(\mathrm{i}a_0)$

$$\begin{aligned}&(\mathrm{i}a_0)^2(C_\infty^2-1)+(\mathrm{i}a_0)(2C_\infty K_\infty-C_\infty)+(K_\infty^2-\lambda^2\\&\quad-2((\mathrm{i}a_0)C_\infty+K_\infty)(Y^{(1)}(a_0))^{-1}+(Y^{(1)}(a_0))^{-2}-a_0(Y^{(1)}(a_0))^{-2}Y^{(1)}(a_0)_{,a_0})=0\end{aligned} \tag{73}$$

DOI: 10.1002/nme

This equation is satisfied by setting each term to zero in descending order of $(\mathrm{i}a_0)$. The $(\mathrm{i}a_0)^2$ term leads to an equation of C_∞. Its positive solution (satisfying the radiation condition) is equal to

$$C_\infty = 1 \tag{74}$$

The $(\mathrm{i}a_0)$ term leads to an equation of K_∞. By using Equation (74), its solution is expressed as

$$K_\infty = 0.5 \tag{75}$$

The remaining term is an equation of $Y^{(1)}(a_0)$ representing the residual

$$K_\infty^2 - \lambda^2 - 2((\mathrm{i}a_0)C_\infty + K_\infty)(Y^{(1)}(a_0))^{-1} + (Y^{(1)}(a_0))^{-2} - a_0(Y^{(1)}(a_0))^{-2}Y^{(1)}(a_0)_{,a_0} = 0 \tag{76}$$

Equation (76) is simplified by multiplying it with $(Y^{(1)}(a_0))^2$ and using the solutions of C_∞ (Equation (74)) and K_∞ (Equation (75)). To construct a recursive procedure, the resulting equation is expressed as the $i=1$ case of

$$a^{(i)} - 2(b_0^{(i)} + (\mathrm{i}a_0))Y^{(i)}(a_0) + c^{(i)}(Y^{(i)}(a_0))^2 - a_0(Y^{(i)}(a_0))_{,a_0} = 0 \tag{77}$$

with the coefficients defined as

$$a^{(1)} = 1 \tag{78a}$$

$$b_0^{(1)} = 0.5 \tag{78b}$$

$$c^{(1)} = 0.25 - \lambda^2 \tag{78c}$$

A recursive equation for determining the remaining constants in the continued fraction solution is obtained by substituting Equation (72b) into Equation (77)

$$\begin{aligned}
&(\mathrm{i}a_0)^2(-2Y_1^{(i)} + c^{(i)}(Y_1^{(i)})^2) + (\mathrm{i}a_0)(-2Y_0^{(i)} - 2b_0^{(i)}Y_1^{(i)} + 2c^{(i)}Y_0^{(i)}Y_1^{(i)} - Y_1^{(i)}) \\
&\quad + (a^{(i)} - 2b_0^{(i)}Y_0^{(i)} + c^{(i)}(Y_0^{(i)})^2 + (-2c^{(i)}(Y_0^{(i)} + (\mathrm{i}a_0)Y_1^{(i)}) + 2((\mathrm{i}a_0) + b_0^{(i)}))(Y^{(i+1)}(a_0))^{-1} \\
&\quad + c^{(i)}(Y^{(i+1)}(a_0))^{-2} - (Y^{(i+1)}(a_0))^{-2}a_0(Y^{(i+1)}(a_0))_{,a_0}) = 0
\end{aligned} \tag{79}$$

This series equation in terms of $(\mathrm{i}a_0)$ is satisfied by setting the individual terms to zero in descending order of $(\mathrm{i}a_0)$. The $(\mathrm{i}a_0)^2$ term leads to an equation of $Y_1^{(i)}$. Its non-zero solution is equal to

$$Y_1^{(i)} = 2/c^{(i)} \tag{80}$$

Setting the $(\mathrm{i}a_0)$ term in Equation (79) to zero yields an equation of $Y_0^{(i)}$. By using Equation (80), its solution is obtained as

$$Y_0^{(i)} = (2b_0^{(i)} + 1)/c^{(i)} \tag{81}$$

The remaining term is written as

$$\begin{aligned}
&a^{(i)} + Y_0^{(i)} - 2(c^{(i)}Y_0^{(i)} - b_0^{(i)} + (\mathrm{i}a_0)(c^{(i)}Y_1^{(i)} - 1))(Y^{(i+1)}(a_0))^{-1} \\
&\quad + c^{(i)}(Y^{(i+1)}(a_0))^{-2} - (Y^{(i+1)}(a_0))^{-2}a_0(Y^{(i+1)}(a_0))_{,a_0} = 0
\end{aligned} \tag{82}$$

DOI: 10.1002/nme

Using Equations (80) and (81), Equation (82) is rewritten as an equation of $Y^{(i+1)}(a_0)$

$$c^{(i)} - 2(b_0^{(i)} + 1 + (\mathrm{i}a_0))Y^{(i+1)}(a_0) + (a^{(i)} + Y_0^{(i)})(Y^{(i+1)}(a_0))^2 - a_0(Y^{(i+1)}(a_0))_{,a_0} = 0 \tag{83}$$

Introducing the recursive formula for the following coefficients:

$$a^{(i+1)} = c^{(i)} \tag{84a}$$

$$b_0^{(i+1)} = b_0^{(i)} + 1 \tag{84b}$$

$$c^{(i+1)} = a^{(i)} + Y_0^{(i)} \tag{84c}$$

Equation (83) is formulated as the $i+1$ case of Equation (77). The constants $Y_1^{(i)}$ and $Y_0^{(i)}$ $(i = 1, 2, \ldots, M_{\mathrm{H}})$ of the singly asymptotic continued fraction solution are thus determined recursively. By combining Equations (78b) and (84b), the constant $b_0^{(i)}$ can be expressed explicitly as

$$b_0^{(i)} = i - 0.5 \tag{85}$$

For later use, the following identity is derived from Equations (84), (81) and (78)

$$(b_0^{(i+1)})^2 - a^{(i+1)}c^{(i+1)} = (b_0^{(i)} + 1)^2 - c^{(i)}a^{(i)} - c^{(i)}Y_0^{(i)} = (b_0^{(i)})^2 - a^{(i)}c^{(i)} = \lambda^2 \tag{86}$$

As an example, the constants of the order $M_{\mathrm{H}} = 2$ continued fraction solution are evaluated

$$Y_0^{(1)} = \frac{8}{1 - 4\lambda^2}, \quad Y_1^{(1)} = \frac{8}{1 - 4\lambda^2} \tag{87a}$$

$$Y_0^{(2)} = \frac{4 - 16\lambda^2}{9 - 4\lambda^2}, \quad Y_1^{(2)} = \frac{2 - 8\lambda^2}{9 - 4\lambda^2} \tag{87b}$$

Together with the constants C_∞ and K_∞ given in Equations (74) and (75), the single-asymptotic solution is obtained after neglecting $(Y^{(3)}(a_0))^{-1}$. The normalized dynamic stiffness coefficient $S(a_0)/\lambda$ of mode $\lambda = 20$ is plotted as a function of the dimensionless frequency a_0/λ in Figure 6. Although it is highly accurate at high frequencies $(a_0/\lambda > 1.25)$, the error increases as the frequency

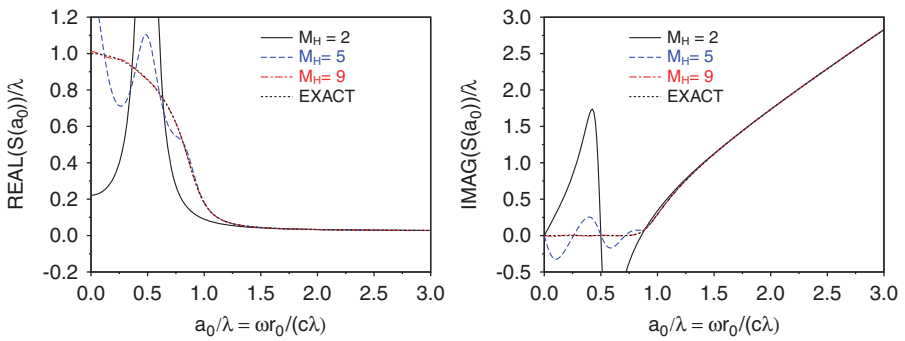

Figure 6. High-frequency continued fraction solution for dynamic stiffness coefficient of circular cavity $(\lambda = 20)$.

DOI: 10.1002/nme

becomes lower. Below the frequency $a_0/\lambda<1$, very large error exists. Unlike the case of the semi-infinite layer, the singly asymptotic solution converges to the exact solution over the whole range of frequency. As shown in Figure 6, an accurate result is obtained at the order $M_H=9$. The rate of convergence close to $a_0=0$ is much slower than that at the high-frequency range. As it will be demonstrated in Section 5.2, the rate of convergence deteriorates as the modal eigenvalue increases.

3.2.2. Doubly asymptotic continued fraction. $Y^{(M_H+1)}(a_0)$ represents the residual of the order M_H high-frequency continued fraction. It satisfies Equation (83) with $i=M_H$ and the coefficients in Equation (84). To facilitate the derivation of the low-frequency continued fraction solution, Equation (83) is rewritten as

$$a_L-2(b_{L0}+(\mathrm{i}a_0))Y_L(a_0)+c_L(Y_L(a_0))^2-a_0(Y_L(a_0))_{,a_0}=0 \tag{88}$$

where the function is

$$Y_L(a_0)=Y^{(M_H+1)}(a_0) \tag{89}$$

and the constants are

$$a_L=a^{(M_H+1)} \tag{90a}$$

$$b_{L0}=b_0^{(M_H+1)}=M_H+0.5 \tag{90b}$$

$$c_L=c^{(M_H+1)} \tag{90c}$$

The continued fraction solution at low frequencies is expressed as

$$Y_L(a_0)=Y_{L0}^{(0)}+(\mathrm{i}a_0)Y_{L1}^{(0)}-(\mathrm{i}a_0)^2(Y_L^{(1)}(a_0))^{-1} \tag{91a}$$

$$Y_L^{(i)}(a_0)=Y_{L0}^{(i)}+(\mathrm{i}a_0)Y_{L1}^{(i)}-(\mathrm{i}a_0)^2(Y_L^{(i+1)}(a_0))^{-1} \quad (i=1,2,\ldots,M_L) \tag{91b}$$

Substituting Equation (91a) into Equation (88) yields an equation in terms of a power series of $(\mathrm{i}a_0)$

$$\begin{aligned}&(a_L-2b_{L0}Y_{L0}^{(0)}+c_L(Y_{L0}^{(0)})^2)+(\mathrm{i}a_0)(-2Y_{L0}^{(0)}-2b_{L0}Y_{L1}^{(0)}+2c_LY_{L0}^{(0)}Y_{L1}^{(0)}-Y_{L1}^{(0)})\\&+(\mathrm{i}a_0)^2(-2Y_{L1}^{(0)}+c_L(Y_{L1}^{(0)})^2+(2(b_{L0}+(\mathrm{i}a_0))-2c_L(Y_{L0}^{(0)}+(\mathrm{i}a_0)Y_{L1}^{(0)}))(Y_L^{(1)}(a_0))^{-1}\\&+2(Y_L^{(1)}(a_0))^{-1}+(\mathrm{i}a_0)^2c_L(Y_L^{(1)}(a_0))^{-2}-(Y_L^{(1)}(a_0))^{-2}a_0(Y_L^{(1)}(a_0))_{,a_0})=0\end{aligned} \tag{92}$$

It is satisfied by setting the terms to zero in ascending order of $(\mathrm{i}a_0)$. The constant term yields

$$a_L-2b_{L0}Y_{L0}^{(0)}+c_L(Y_{L0}^{(0)})^2=0 \tag{93}$$

By using Equations (86) and (90), the determinant of this quadratic algebraic equation is equal to

$$(2b_{L0})^2-4a_Lc_L=4\lambda^2 \tag{94}$$

The solution for $Y_{L0}^{(0)}$ is expressed as

$$Y_{L0}^{(0)}=(b_{L0}+\lambda)/c_L=(M_H+0.5+\lambda)/c_L \tag{95}$$

DOI: 10.1002/nme

Setting the $(\mathrm{i}a_0)$ term of Equation (92) to zero leads to an equation of $Y_{\mathrm{L1}}^{(0)}$. By using Equation (95), its solution is equal to

$$Y_{\mathrm{L1}}^{(0)} = 2Y_{\mathrm{L0}}^{(0)}/(2\lambda - 1) \tag{96}$$

Setting the remaining term of Equation (92) to zero results in an equation of $Y_{\mathrm{L}}^{(1)}(a_0)$. It is denoted as the $i = 1$ case of

$$(\mathrm{i}a_0)^2 a_{\mathrm{L}}^{(i)} - 2(b_{\mathrm{L0}}^{(i)} + b_{\mathrm{L1}}^{(i)}(\mathrm{i}a_0))Y_{\mathrm{L}}^{(i)}(a_0) + c_{\mathrm{L}}^{(i)}(Y_{\mathrm{L}}^{(i)}(a_0))^2 - a_0(Y_{\mathrm{L}}^{(i)}(a_0))_{,a_0} = 0 \tag{97}$$

where the following constants are defined and simplified using Equations (95) and (96) as:

$$a_{\mathrm{L}}^{(1)} = c_{\mathrm{L}} \tag{98a}$$

$$b_{\mathrm{L0}}^{(1)} = -1 - b_{\mathrm{L0}} + c_{\mathrm{L}} Y_{\mathrm{L0}}^{(0)} = -1 + \lambda \tag{98b}$$

$$b_{\mathrm{L1}}^{(1)} = -1 + c_{\mathrm{L}} Y_{\mathrm{L1}}^{(0)} = 2(M_{\mathrm{H}} + 1)/(2\lambda - 1) \tag{98c}$$

$$c_{\mathrm{L}}^{(1)} = -2Y_{\mathrm{L1}}^{(0)} + c_{\mathrm{L}}(Y_{\mathrm{L1}}^{(0)})^2 \tag{98d}$$

Substituting Equation (91b) into Equation (97) results in an equation in terms of a power series of $(\mathrm{i}a)$

$$\begin{aligned}
&(-2b_{\mathrm{L0}}^{(i)}Y_{\mathrm{L0}}^{(i)} + c_{\mathrm{L}}^{(i)}(Y_{\mathrm{L0}}^{(i)})^2) + (\mathrm{i}a_0)(-2(b_{\mathrm{L1}}^{(i)}Y_{\mathrm{L0}}^{(i)} + b_{\mathrm{L0}}^{(i)}Y_{\mathrm{L1}}^{(i)}) + 2c_{\mathrm{L}}^{(i)}Y_{\mathrm{L0}}^{(i)}Y_{\mathrm{L1}}^{(i)} - Y_{\mathrm{L1}}^{(i)}) \\
&\quad + (\mathrm{i}a_0)^2(a_{\mathrm{L}}^{(i)} - 2b_{\mathrm{L1}}^{(i)}Y_{\mathrm{L1}}^{(i)} + c_{\mathrm{L}}^{(i)}(Y_{\mathrm{L1}}^{(i)})^2 - 2(-1 - b_{\mathrm{L0}}^{(i)} + c_{\mathrm{L}}^{(i)}Y_{\mathrm{L0}}^{(i)} + (\mathrm{i}a_0) \\
&\quad \times(-b_{\mathrm{L1}}^{(i)} + c_{\mathrm{L}}^{(i)}Y_{\mathrm{L1}}^{(i)}))(Y_{\mathrm{L}}^{(i+1)}(a_0))^{-1} + (\mathrm{i}a_0)^2 c_{\mathrm{L}}^{(i)}(Y_{\mathrm{L}}^{(i+1)}(a_0))^{-2} \\
&\quad -(Y_{\mathrm{L}}^{(i+1)}(a_0))^{-2} a_0(Y_{\mathrm{L}}^{(i+1)}(a_0))_{,a_0}) = 0
\end{aligned} \tag{99}$$

Setting the individual terms to zero in ascending order of $(\mathrm{i}a_0)$ leads to the equations of $Y_{\mathrm{L0}}^{(i)}$, $Y_{\mathrm{L1}}^{(i)}$ and $Y_{\mathrm{L}}^{(i+1)}(a_0)$, respectively. The constant term independent of $(\mathrm{i}a_0)$ yields an equation of $Y_{\mathrm{L0}}^{(i)}$. Its non-zero solution is equal to

$$Y_{\mathrm{L0}}^{(i)} = 2b_{\mathrm{L0}}^{(i)}/c_{\mathrm{L}}^{(i)} \tag{100}$$

The $(\mathrm{i}a_0)$ term is an equation for $Y_{\mathrm{L1}}^{(i)}$. By using Equation (100), its solution is expressed as

$$Y_{\mathrm{L1}}^{(i)} = 2b_{\mathrm{L1}}^{(i)}Y_{\mathrm{L0}}^{(i)}/(-1 + 2b_{\mathrm{L0}}^{(i)}) \tag{101}$$

The last term of Equation (99) results in an equation of $Y_{\mathrm{L}}^{(i+1)}(a_0)$

$$\begin{aligned}
&(\mathrm{i}a_0)^2 c_{\mathrm{L}}^{(i)} - 2(-1 - b_{\mathrm{L0}}^{(i)} + c_{\mathrm{L}}^{(i)}Y_{\mathrm{L0}}^{(i)} + (\mathrm{i}a_0)(-b_{\mathrm{L1}}^{(i)} + c_{\mathrm{L}}^{(i)}Y_{\mathrm{L1}}^{(i)}))Y_{\mathrm{L}}^{(i+1)}(a_0) \\
&\quad + (a_{\mathrm{L}}^{(i)} - 2b_{\mathrm{L1}}^{(i)}Y_{\mathrm{L1}}^{(i)} + c_{\mathrm{L}}^{(i)}(Y_{\mathrm{L1}}^{(i)})^2)(Y_{\mathrm{L}}^{(i+1)}(a_0))^2 - a_0(Y_{\mathrm{L}}^{(i+1)}(a_0))_{,a_0} = 0
\end{aligned} \tag{102}$$

DOI: 10.1002/nme

Introducing the recursive equations

$$a_{\mathrm{L}}^{(i+1)} = c_{\mathrm{L}}^{(i)} \tag{103a}$$

$$b_{\mathrm{L0}}^{(i+1)} = -1 - b_{\mathrm{L0}}^{(i)} + c_{\mathrm{L}}^{(i)} Y_{\mathrm{L0}}^{(i)} = -1 + b_{\mathrm{L0}}^{(i)} \tag{103b}$$

$$b_{\mathrm{L1}}^{(i+1)} = -b_{\mathrm{L1}}^{(i)} + c_{\mathrm{L}}^{(i)} Y_{\mathrm{L1}}^{(i)} \tag{103c}$$

$$c_{\mathrm{L}}^{(i+1)} = a_{\mathrm{L}}^{(i)} - 2b_{\mathrm{L1}}^{(i)} Y_{\mathrm{L1}}^{(i)} + c_{\mathrm{L}}^{(i)} (Y_{\mathrm{L1}}^{(i)})^2 \tag{103d}$$

with the expression of $b_{\mathrm{L0}}^{(i+1)}$ simplified by using Equation (100), Equation (102) is expressed as the $(i+1)$ case of Equation (97). With the combination of Equations (98b) and (103b), the constant $b_{\mathrm{L0}}^{(i)}$ is expressed as

$$b_{\mathrm{L0}}^{(i)} = -i + \lambda \tag{104}$$

The doubly asymptotic solution can now be determined by combining the high-frequency continued fraction solution in Equation (72) with the low-frequency continued fraction solution in Equation (91) using $Y^{(M_{\mathrm{H}}+1)}(a_0) = Y_{\mathrm{L}}(a_0)$ (Equation (88)). As an example, the low-frequency continued fraction is determined for the residual term of the $M_{\mathrm{H}} = 2$ high-frequency continued fraction. The result of order $M_{\mathrm{L}} = 2$ is

$$Y_{\mathrm{L0}}^{(0)} = \frac{18 - 8\lambda^2}{8\lambda^3 - 20\lambda^2 - 2\lambda + 5}, \quad Y_{\mathrm{L1}}^{(0)} = \frac{-4(4\lambda^2 - 9)}{(2\lambda - 1)^2(4\lambda^2 - 8\lambda - 5)} \tag{105a}$$

$$Y_{\mathrm{L0}}^{(1)} = \frac{(\lambda - 1)(2\lambda - 1)^3(4\lambda^2 - 8\lambda - 5)}{2(8\lambda^3 - 28\lambda^2 - 18\lambda + 63)}, \quad Y_{\mathrm{L1}}^{(1)} = \frac{6(\lambda - 1)(2\lambda - 5)(2\lambda - 1)^2(2\lambda + 1)}{(2\lambda - 3)^2(4\lambda^2 - 8\lambda - 21)} \tag{105b}$$

$$Y_{\mathrm{L0}}^{(2)} = \frac{-8(\lambda - 2)(2\lambda - 7)(2\lambda - 3)^3}{(2\lambda - 1)^3(8\lambda^3 - 52\lambda^2 + 62\lambda + 45)}, \quad Y_{\mathrm{L1}}^{(2)} = \frac{-96(\lambda - 2)(2\lambda - 7)(2\lambda - 3)^2}{(2\lambda - 5)^2(2\lambda - 1)^3(4\lambda^2 - 16\lambda - 9)} \tag{105c}$$

The result of the order $M_{\mathrm{H}} = M_{\mathrm{L}} = 2$ doubly asymptotic solution for the mode $\lambda = 20$ is plotted in Figure 7. Compared with the order $M_{\mathrm{H}} = 5$ singly asymptotic solution, which has the same number of terms, the doubly asymptotic solution is much more accurate.

4. IMPLEMENTATION OF CONTINUED FRACTION SOLUTION IN THE TIME DOMAIN

In the frequency domain, the open boundary condition is expressed as the force–displacement relationship (Equations (9) and (26))

$$\widetilde{R} = S(a_0)\widetilde{U} \tag{106}$$

When the dynamic stiffness coefficient $S(a_0)$ is expressed as a continued fraction solution, the force–displacement relationship can be formulated in the time domain as a system of first-order ordinary differential equations with time-independent coefficient matrices, which represents a temporally local open boundary.

DOI: 10.1002/nme

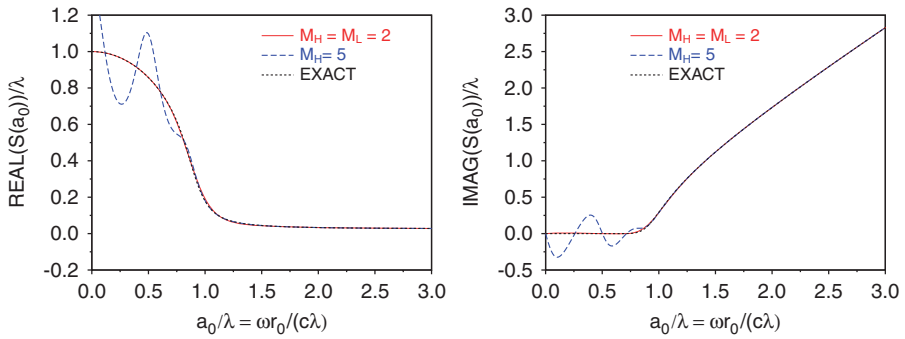

Figure 7. Doubly asymptotic continued fraction solution for dynamic stiffness coefficient of circular cavity ($\lambda = 20$).

A doubly asymptotic continued fraction solution, which includes the expressions for the semi-infinite layer and circular cavity as special cases, is considered

$$S(a_0) = K_\infty + (\mathrm{i}a_0)C_\infty - m^2(Y^{(1)}(a_0))^{-1} \tag{107a}$$

$$Y^{(i)}(a_0) = Y_0^{(i)} + (\mathrm{i}a_0)Y_1^{(i)} - m^2(Y^{(i+1)}(a_0))^{-1} \quad (i = 1, 2, \ldots, M_\mathrm{H}) \tag{107b}$$

$$Y_\mathrm{L}(a_0) = Y^{(M_\mathrm{H}+1)}(a_0) \tag{107c}$$

$$Y_\mathrm{L}(a_0) = Y_{\mathrm{L}0} + (\mathrm{i}a_0)Y_{\mathrm{L}1} - (\mathrm{i}a_0)^2(Y_\mathrm{L}^{(1)}(a_0))^{-1} \tag{107d}$$

$$Y_\mathrm{L}^{(i)}(a_0) = Y_{\mathrm{L}0}^{(i)} + (\mathrm{i}a_0)Y_{\mathrm{L}1}^{(i)} - (\mathrm{i}a_0)^2(Y_\mathrm{L}^{(i+1)}(a_0))^{-1} \quad (i = 1, 2, \ldots, M_\mathrm{L}) \tag{107e}$$

with the dimensionless frequency

$$a_0 = \frac{\omega r_0}{c} \tag{108}$$

For the semi-infinite layer (Equations (37) and (57)), $K_\infty = Y_0^{(i)} = Y_{\mathrm{L}1}^{(i)} = 0$ and $m = \lambda$ applies. The characteristic length r_0 in Equation (108) is replaced with the depth h. For the circular cavity (Equations (72) and (91)), $m = 1$ applies. Substituting Equation (107a) into the force–displacement relationship in Equation (106) leads to

$$\widetilde{R} = S(a_0)\widetilde{U} = K_\infty\widetilde{U} + (\mathrm{i}a_0)C_\infty\widetilde{U} - m\widetilde{U}^{(1)} \tag{109}$$

where the auxiliary variable $\widetilde{U}^{(1)}$ is defined as

$$\widetilde{U}^{(1)} = m(Y^{(1)}(a_0))^{-1}\widetilde{U} \tag{110}$$

and then reformulated as

$$m\widetilde{U} = Y^{(1)}(a_0)\widetilde{U}^{(1)} \tag{111}$$

which is in the same form as the force–displacement relationship (Equation (106)). Similarly, an auxiliary variable is introduced for each term of continued fraction in Equation (107b)

$$m\widetilde{U}^{(i)} = Y^{(i+1)}(a_0)\widetilde{U}^{(i+1)} \quad (i = 0, 1, 2, \ldots, M_\mathrm{H}) \tag{112}$$

DOI: 10.1002/nme

where Equation (111) is included as the $i=0$ case with $\widetilde{U}^{(0)}=\widetilde{U}$. Multiplying Equation (107b) by $\widetilde{U}^{(i)}$ and using the definition of auxiliary variables in Equation (112) formulated at i and $i-1$ result in

$$m\widetilde{U}^{(i-1)}=Y_0^{(i)}\widetilde{U}^{(i)}+(\mathrm{i}a_0)Y_1^{(i)}\widetilde{U}^{(i)}-m\widetilde{U}^{(i+1)} \quad (i=1,2,\ldots,M_{\mathrm{H}}) \tag{113}$$

The residual $\widetilde{U}^{(M_{\mathrm{H}}+1)}$ of an order M_{H} high-frequency continued fraction solution is expressed in Equation (112) at $i=M_{\mathrm{H}}$ as

$$m\widetilde{U}^{(M_{\mathrm{H}})}=Y^{(M_{\mathrm{H}}+1)}(a_0)\widetilde{U}^{(M_{\mathrm{H}}+1)} \tag{114}$$

$Y^{(M_{\mathrm{H}}+1)}=Y_{\mathrm{L}}(a_0)$ (Equation (107c)) is expressed in Equation (107d) as a low-frequency continued fraction solution. Multiplying Equation (107d) by $\widetilde{U}^{(M_{\mathrm{H}}+1)}$ and using Equations (107c) and (114) lead to

$$m\widetilde{U}^{(M_{\mathrm{H}})}=Y_{\mathrm{L}0}\widetilde{U}^{(M_{\mathrm{H}}+1)}+(\mathrm{i}a_0)Y_{\mathrm{L}1}\widetilde{U}^{(M_{\mathrm{H}}+1)}-(\mathrm{i}a_0)\widetilde{U}_{\mathrm{L}}^{(1)} \tag{115}$$

where the auxiliary variable $\widetilde{U}_{\mathrm{L}}^{(1)}$ is defined in

$$(\mathrm{i}a_0)\widetilde{U}^{(M_{\mathrm{H}}+1)}=Y_{\mathrm{L}}^{(1)}(a_0)\widetilde{U}_{\mathrm{L}}^{(1)} \tag{116}$$

Again, an auxiliary variable is introduced for each term of the continued fraction in Equation (107e) as

$$(\mathrm{i}a_0)\widetilde{U}_{\mathrm{L}}^{(i)}=Y_{\mathrm{L}}^{(i+1)}(a_0)\widetilde{U}_{\mathrm{L}}^{(i+1)} \quad (i=0,1,2,\ldots,M_{\mathrm{L}}) \tag{117}$$

with $\widetilde{U}_{\mathrm{L}}^{(0)}=\widetilde{U}^{(M_{\mathrm{H}}+1)}$. Multiplying Equation (107e) by $\widetilde{U}_{\mathrm{L}}^{(i)}$ and using Equation (117) at $i-1$ and i yield

$$(\mathrm{i}a_0)\widetilde{U}_{\mathrm{L}}^{(i-1)}=Y_{\mathrm{L}0}^{(i)}\widetilde{U}_{\mathrm{L}}^{(i)}+(\mathrm{i}a_0)Y_{\mathrm{L}1}^{(i)}\widetilde{U}_{\mathrm{L}}^{(i)}-(\mathrm{i}a_0)\widetilde{U}_{\mathrm{L}}^{(i+1)} \quad (i=1,2,\ldots,M_{\mathrm{L}}) \tag{118}$$

For the order M_{L} low-frequency solution, the approximation $\widetilde{U}_{\mathrm{L}}^{(M_{\mathrm{L}}+1)}=0$ is introduced.

Equations (109), (113), (115) and (118) are all combined to form a matrix equation

$$([K_h]+\mathrm{i}\omega[C_h])\{Z\}=\{F\} \tag{119}$$

with

$$\{Z\}=[\widetilde{U},\widetilde{U}^{(1)},\ldots,\widetilde{U}^{(M_{\mathrm{H}})},\widetilde{U}^{(M_{\mathrm{H}}+1)},\widetilde{U}_{\mathrm{L}}^{(1)},\ldots,\widetilde{U}_{\mathrm{L}}^{(M_{\mathrm{L}})}]^{\mathrm{T}} \tag{120a}$$

$$\{F\}=[\widetilde{R},0,\ldots,0,0,0,\ldots,0]^{\mathrm{T}} \tag{120b}$$

DOI: 10.1002/nme

$$[K_h]=\begin{bmatrix} K_\infty & -m & & & & & & \\ -m & Y_0^{(1)} & \ddots & & & & & \\ & \ddots & \ddots & -m & & & & \\ & & -m & Y_0^{(M_H)} & -m & & & \\ & & & -m & Y_{L0} & 0 & & \\ & & & & 0 & Y_{L0}^{(1)} & \ddots & \\ & & & & & \ddots & \ddots & 0 \\ & & & & & & 0 & Y_{L0}^{(M_L)} \end{bmatrix} \tag{120c}$$

$$[C_h]=\frac{r_0}{c}\begin{bmatrix} C_\infty & 0 & & & & & & \\ 0 & Y_1^{(1)} & \ddots & & & & & \\ & \ddots & \ddots & 0 & & & & \\ & & 0 & Y_1^{(M_H)} & 0 & & & \\ & & & 0 & Y_{L1} & -1 & & \\ & & & & -1 & Y_{L1}^{(1)} & \ddots & \\ & & & & & \ddots & \ddots & -1 \\ & & & & & & -1 & Y_{L1}^{(M_L)} \end{bmatrix} \tag{120d}$$

The function $\{Z\}$ includes the displacement amplitude on the boundary and all the auxiliary variables, and the only non-zero entry at the right-hand side $\{F\}$ is the excitation force $\widetilde{R}$ on the boundary. Note that Equation (108) is substituted into the equation to replace ia_0 with $i\omega$. The time-independent matrices $[K_h]$ and $[C_h]$ are tri-diagonal and symmetric. Equation (119) is expressed in the time domain as

$$[K_h]\{z(t)\}+[C_h]\{\dot{z}(t)\}=\{f(t)\} \tag{121}$$

It represents a temporally local high-order open boundary applicable to one mode of wave propagation in a semi-infinite layer with a constant depth or a circular cavity in a full-plane.

This paper is limited to develop and evaluate the high-order open boundary for one mode of wave propagation. The implementation of such an open boundary in the finite element method has been well documented, for example, in References [29, 44] and will not be repeated herein.

DOI: 10.1002/nme

5. NUMERICAL EXAMPLES

The accuracy of the proposed doubly asymptotic open boundaries is evaluated in this section. Newmark's method with $\gamma=0.5$ and $\beta=0.25$ (average acceleration scheme) is employed for the time integration. The size of the time step is chosen as $\Delta t=0.01h/(\lambda c)$ for the semi-infinite layer and $\Delta t=0.01r_0/(\lambda c)$ for the circular cavity.

When the present doubly asymptotic open boundary is employed, the only two parameters for the users to select are the orders of high- and low-frequency continued fractions M_{H} and M_{L}. In this paper, the same value is chosen for both parameters. With this simple, although not necessarily optimal, choice, the doubly asymptotic open boundaries perform much better than the singly asymptotic open boundaries with the same number of terms do.

The excitation by a unit impulse of traction $\tilde{\tau}_{0I}(t)=\delta(t)$ is chosen to evaluate the accuracy of open boundaries as it covers the whole frequency range. When a unit impulse is applied, the initial condition is obtained by integrating Equation (121) with the matrix $[C_h]$ given in Equation (120d). (Note that the first entry of $\{f(t)\}$ and $\{z(t)\}$ is $\tilde{\tau}_{0I}(t)$ and $\tilde{u}(t)$, respectively.)

$$\tilde{u}(t=0)=c/(r_0C_\infty) \tag{122}$$

In the case of semi-infinite layer, r_0 in Equation (122) is replaced with the depth h of the layer.

To investigate the performance of the open boundary at a specified frequency range, the surface traction is prescribed as a Ricker wavelet. The time history of the Ricker wavelet is given as

$$\tilde{\tau}_0(t)=A_{\mathrm{R}}\left(1-2\left(\frac{t-t_s}{t_0}\right)^2\right)\exp\left(-\left(\frac{t-t_s}{t_0}\right)^2\right) \tag{123}$$

where t_s is the time when the wavelet reaches its maximum, $2/t_0$ is the dominant angular frequency of the wavelet and A_{R} is the amplitude. The Fourier transform of the wavelet is expressed as

$$\tilde{R}_0(\omega)=0.5\sqrt{\pi}A_{\mathrm{R}}t_0(\omega t_0)^2\mathrm{e}^{-0.25(\omega t_0)^2} \tag{124}$$

A Ricker wavelet with the parameters $\bar{t}_s=ct_s/h=1$, $\bar{t}_0=ct_0/h=0.2$ and $A_{\mathrm{R}}=10$ is shown in Figure 8(a). The amplitude of its Fourier transform is plotted in Figure 8(b). The dominant dimensionless frequency of this wavelet is $a_0=10$.

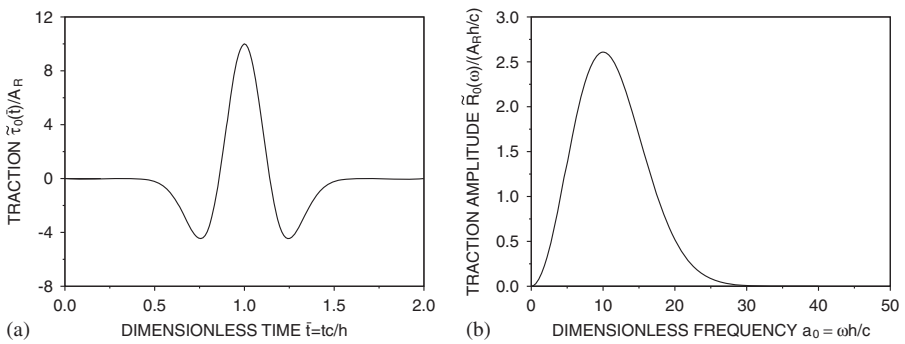

Figure 8. Prescribed traction as a Ricker wavelet: (a) time history and (b) Fourier transform.

DOI: 10.1002/nme

5.1. *Semi-infinite layer with constant depth*

The case of a semi-infinite layer with a constant depth is a stringent test due to the existence of a cut-off frequency. Since the dynamic stiffness is not smooth at the cut-off frequency, this case is especially challenging for the doubly asymptotic continued fraction solution. At the cut-off frequency, the dynamic stiffness is equal to zero. As a result, waves around the cut-off frequency decay at a very slow rate (Equation (14)). This requires that an open boundary has to be accurate over a large time duration. The investigation of the semi-infinite layer is also significant because the construction of several higher-order open boundaries is related to this case as shown in Section 3.1.2.

The performance of the singly asymptotic open boundary based solely on the high-frequency continued fraction solution is evaluated at first. The dynamic stiffness coefficient of the order $M_H=5$ continued fraction is plotted in Figure 4. The cut-off frequency exists at $a_0/\lambda=1$. The large error of the dynamic stiffness coefficient below the cut-off frequency ($a_0/\lambda<1$) indicates that the high-order singly asymptotic open boundary is unable to transmit evanescent waves. This is confirmed by the unit-impulse response of the $M_H=5$ open boundary plotted in Figure 9. The early-time (high-frequency) response is very accurate. The response after the dimensionless time

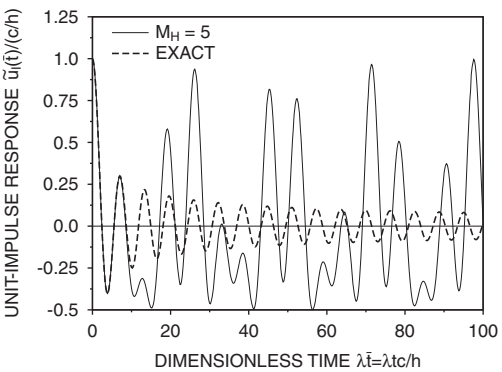

Figure 9. Unit-impulse response of semi-infinite layer by singly asymptotic boundary: $M_H=5$.

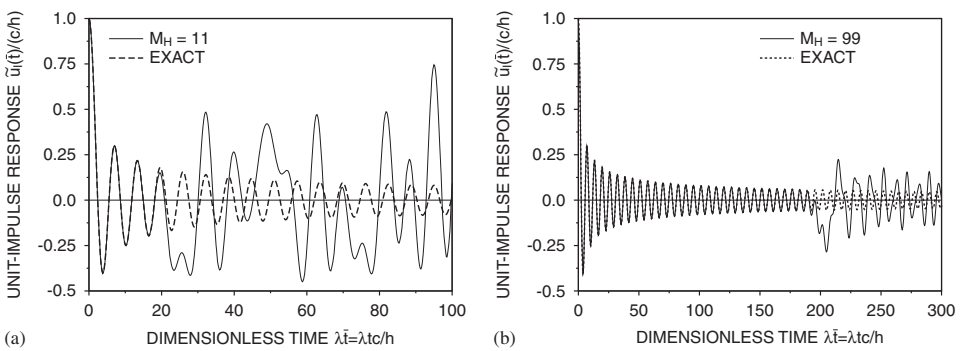

Figure 10. Unit-impulse response of semi-infinite layer by singly asymptotic boundary: (a) $M_H=11$ and (b) $M_H=99$.

DOI: 10.1002/nme

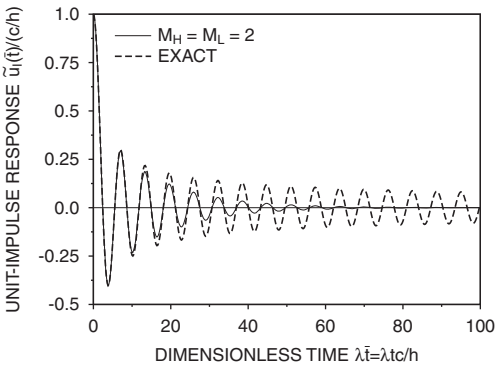

Figure 11. Unit-impulse response of semi-infinite layer by doubly asymptotic boundary: $M_H = M_L = 2$.

$\lambda\bar{t} > 10$ suddenly exhibits a very large error and the amplitude of the error does not decay with time. Since this phenomenon is very similar to fictitious reflections caused by enforcing a simple (free or fixed) boundary condition at a certain distance, it is referred to as 'fictitious reflections' in this paper.

The effect of the order of the singly asymptotic open boundary on its accuracy is also investigated by considering the orders $M_H = 11$ and $M_H = 99$. The order $M_H = 11$ continued fraction solution has 12 terms (double the number of terms of the $M_H = 5$ solution). The order $M_H = 99$ solution has 100 terms. The dynamic stiffness coefficients of both open boundaries are indistinguishable from the exact solution above the cut-off frequency as shown in Figure 4 for the $M_H = 11$ solution (the dynamic stiffness coefficient of the $M_H = 99$ open boundary is not plotted). The unit-impulse responses of both open boundaries are shown in Figure 10. As the order increases, the accuracy improves. However, significant 'fictitious reflections' still occur, albeit at later time, even at order $M_H = 99$. As the amplitude of the 'fictitious reflections' does not decay with time, the singly asymptotic open boundary is unsuitable for the analysis of long-time response.

The defect of the singly asymptotic open boundary in representing low-frequency responses can be mended by employing the doubly asymptotic continued fraction solution in Section 3.1.3. The corresponding higher-order doubly asymptotic open boundary is constructed in Section 4. For the $M_H = M_L = 2$ doubly asymptotic open boundary, whose dynamic stiffness coefficient is shown in Figure 5, the unit-impulse response is plotted in Figure 11. It decays gradually and no 'fictitious reflection' appears. It is observed by comparing Figure 11 with Figure 9 that the $M_H = M_L = 2$ open boundary is much more accurate than the $M_H = 5$ open boundary after $\lambda\bar{t} > 10$, although the number of equations of both formulations is equal to 5.

The accuracy of the doubly asymptotic open boundary improves rapidly as its order increases. This is demonstrated by using the order $M_H = M_L = 5$ open boundary. Its dynamic stiffness coefficient is plotted in Figure 12. It is indistinguishable from the exact solution except for the slight difference close to the cut-off frequency. The unit-impulse response is shown in Figure 13. Good agreement with the exact solution is observed for about the first 10 periods. Compared with the unit-impulse response of the $M_H = 11$ open boundary, which has the same number of variables, in Figure 10(a), the doubly asymptotic open boundary is significantly more accurate at late time. No 'fictitious reflection' occurs.

DOI: 10.1002/nme

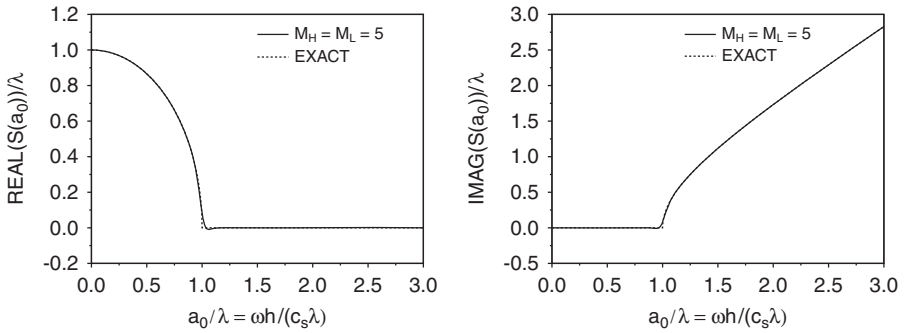

Figure 12. Doubly asymptotic continued fraction solution for dynamic stiffness coefficient of semi-infinite layer: $M_{\mathrm{H}}=M_{\mathrm{L}}=5$.

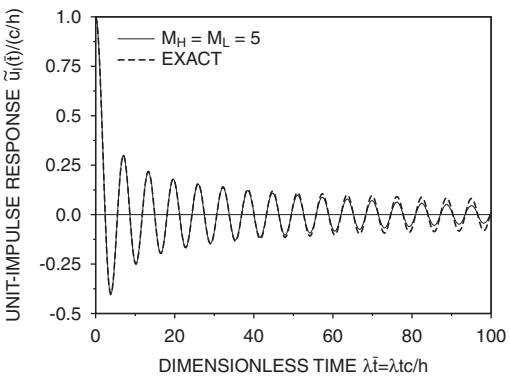

Figure 13. Unit-impulse response of semi-infinite layer by doubly asymptotic boundary: $M_{\mathrm{H}}=M_{\mathrm{L}}=5$.

To further investigate the convergence of the doubly asymptotic open boundary, a long-time analysis, with a duration of $\lambda tc/h=200\pi$, of the unit-impulse response is performed. As the period of the asymptotic solution of the unit-impulse response is $\lambda tc/h=2\pi$, this duration corresponds to 100 periods of vibration. The amplitude of the unit-impulse response decays from 1 at $t=0$ to about 0.032. The result of the $M_{\mathrm{H}}=M_{\mathrm{L}}=24$ open boundary is plotted in Figure 14(a). The unit-impulse response decays gradually and no 'fictitious reflections' occur. The numerical result is indistinguishable from the exact solution at the early stage (Figure 14(b)) and in the middle of the duration (Figure 14(c)). At the end of the duration, the error is merely about 0.0015. Thus, the $M_{\mathrm{H}}=M_{\mathrm{L}}=24$ open boundary is sufficiently accurate for most engineering applications.

The response to a surface traction prescribed as the Ricker wavelet shown in Figure 8 ($\bar{t}_s=ct_s/h=1$, $\bar{t}_0=ct_0/h=0.2$) is computed for three modes $\lambda=5$, 10 and 15. It is similar to the analysis of the semi-infinite layer by using modal superposition. The same amplitude of surface traction $A_{\mathrm{R}}=10$ is assumed for all the three modes. The ratios between the dominate dimensionless frequencies to the modal eigenvalues are $a_0/\lambda=2$, 1 and $\frac{2}{3}$, respectively. The responses of the $M_{\mathrm{H}}=M_{\mathrm{L}}=24$ doubly asymptotic open boundary are plotted in Figure 15. Very good agreement is observed for all the three modes. For comparison, the responses of the $M_{\mathrm{H}}=99$ singly asymptotic

DOI: 10.1002/nme

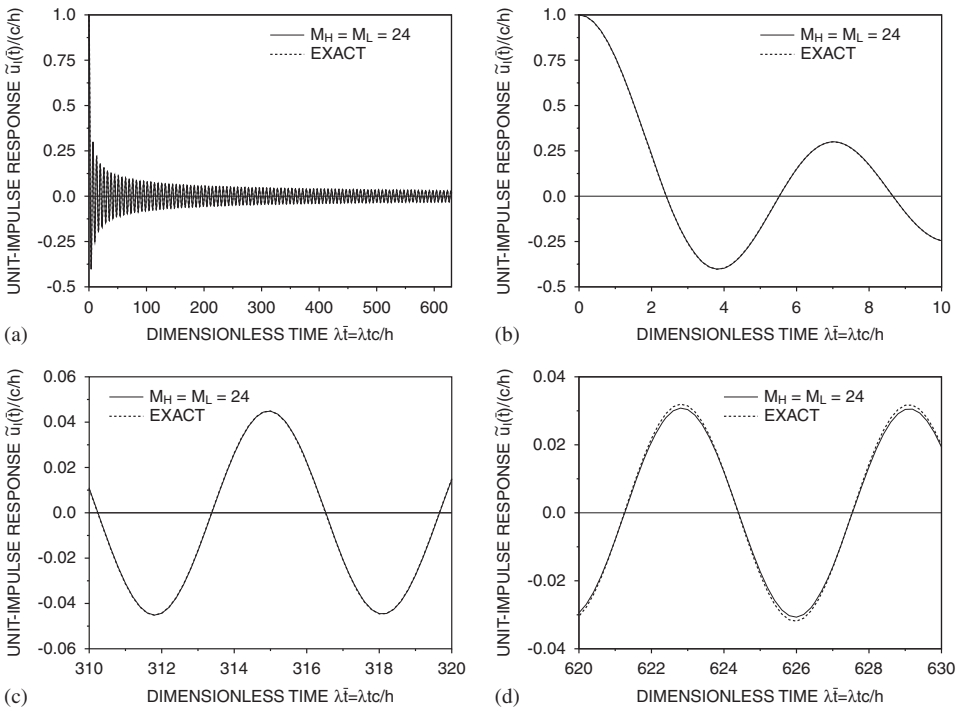

Figure 14. Unit-impulse response of semi-infinite layer by doubly asymptotic boundary: $M_H = M_L = 24$.

open boundary are also shown. As its dynamic stiffness coefficient is very accurate above the cut-off frequency ($a_0 > \lambda$), the response for the mode $\lambda = 5$ (the ratio $a_0/\lambda = 2$) is very accurate (Figure 15(a)) with only a small error after $\bar{t} > 45$. As the mode increases, the 'fictitious reflections' appear. For the mode $\lambda = 15$ (the ratio $a_0/\lambda = 0.5$), the amplitude of the 'fictitious reflections' is very large. In addition, the 'fictitious reflections' arrive earlier as the modal eigenvalue increases.

5.2. Circular cavity embedded in full-plane

As shown in Reference [40], the high-frequency continued fraction solution for the dynamic stiffness coefficient converges to the exact solution for a circular cavity. As the modal eigenvalue increases, the rate of convergence decreases. This is consistent with the observation in References [29, 45] that the accuracy of high-order open boundaries deteriorates as the modal eigenvalue increases.

It has been shown in Section 5.1 for the semi-infinite layer case that the doubly asymptotic high-order open boundary can effectively eliminate the 'fictitious reflections' occurring in the singly asymptotic open boundary. As illustrated in Section 2.3, the dynamic stiffness coefficient of a mode of the circular cavity approaches that of the semi-infinite layer as the modal eigenvalue increases. It is thus expected that the same advantage of the high-order doubly asymptotic open boundary exists when a mode of circular wave with a large eigenvalue is analyzed.

The mode $\lambda = 200$ is, for example, addressed. The dynamic stiffness coefficient of the $M_H = M_L = 5$ open boundary is shown in Figure 16. Excellent agreement with the exact solution

DOI: 10.1002/nme

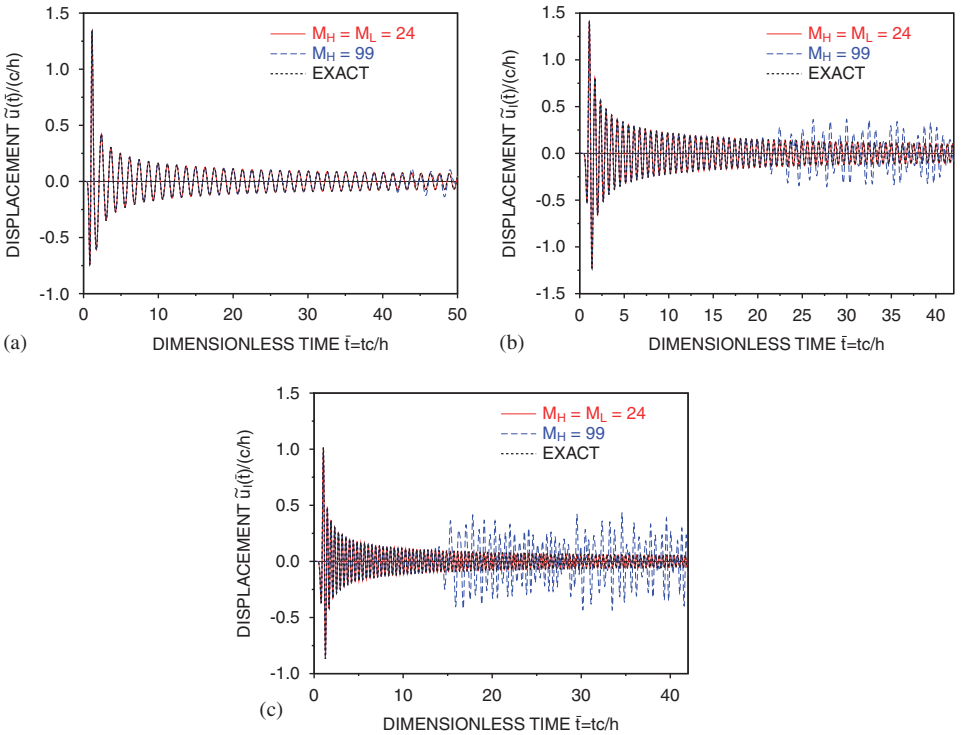

Figure 15. Response of semi-infinite layer to traction varying as Ricker wavelets by $M_{\mathrm{H}} = M_{\mathrm{L}} = 24$ doubly asymptotic boundary: (a) $\lambda = 5$; (b) $\lambda = 10$; and (c) $\lambda = 15$.

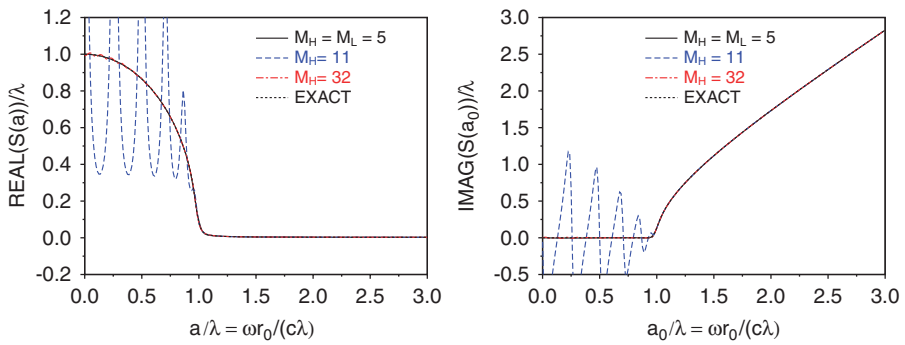

Figure 16. Dynamic stiffness coefficient of circular cavity ($\lambda = 200$).

is obtained. The singly asymptotic continued fraction solution with the same number of terms ($M_{\mathrm{H}} = 11$) leads to a significant error below the cut-off frequency. Only when the order is higher than 32, the singly asymptotic solution is accurate over the whole frequency range. The same is also observed for the unit-impulse response plotted in Figure 17.

DOI: 10.1002/nme

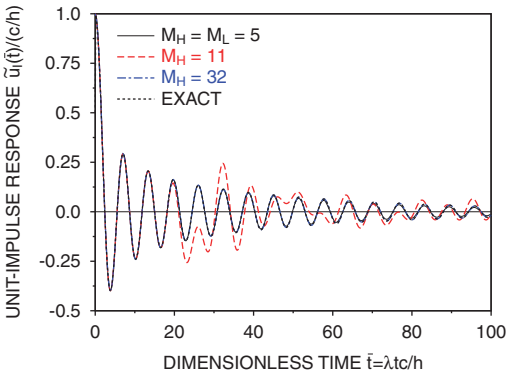

Figure 17. Unit-impulse response of circular cavity ($\lambda = 200$).

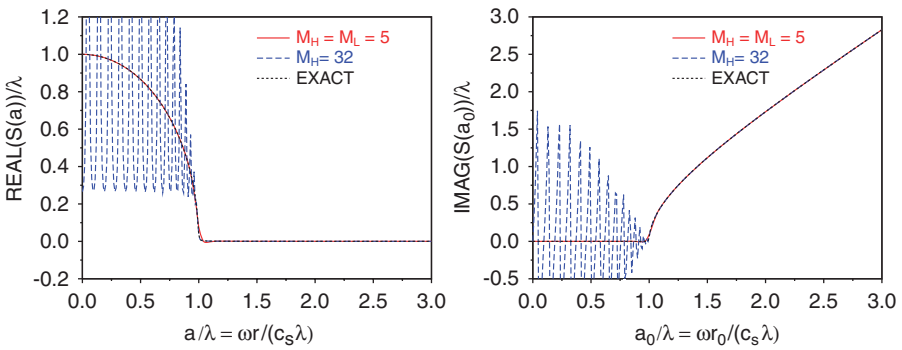

Figure 18. Dynamic stiffness coefficient of circular cavity ($\lambda = 2000$).

The dynamic stiffness coefficient of the mode $\lambda = 2000$ is plotted in Figure 18. As expected, the accuracy of the singly asymptotic solution deteriorates when the modal eigenvalue increases. The result of the order $M_H = 32$ high-frequency continued fraction solution shows strong oscillation below the cut-off frequency. In contrast, the result of the order $M_H = M_L = 5$ doubly asymptotic continued fraction solution is still very close to the exact solution. Only slight difference is observed close to the cut-off frequency. Higher accuracy of doubly asymptotic open boundary is also observed in the unit-impulse response as shown in Figure 19. No 'fictitious reflections' occur.

The response to a surface traction prescribed as the Ricker wavelet is evaluated. The parameters in Equation (123) are chosen as $\bar{t}_s = ct_s/h = 0.01$ and $\bar{t}_0 = ct_0/h = 0.002$. The dominant dimensionless frequency is equal to $a_0 = 1000$, which corresponds to the period of $\overline{T} = 0.002\pi$. The results of open boundaries for the modes $\lambda = 200$ and 2000 are compared with the exact solutions in Figure 20. For the mode $\lambda = 200$, the ratio of dominant dimensionless frequency a_0 to the eigenvalue $\lambda = 200$ is equal to $a_0/\lambda = 5$. As shown in Figure 18, both the $M_H = 32$ singly asymptotic solution and the $M_H = M_L = 5$ doubly asymptotic solution are highly accurate around this frequency. The responses of both open boundaries agree very well with the exact solution as shown in Figure 20(a).

DOI: 10.1002/nme

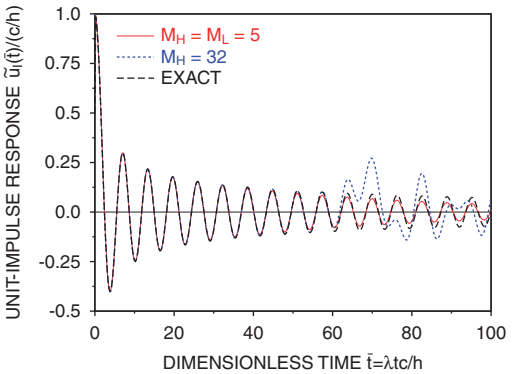

Figure 19. Unit-impulse response of circular cavity ($\lambda = 2000$).

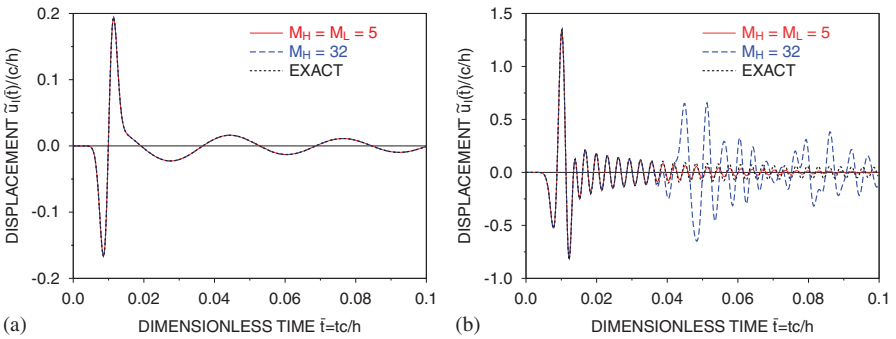

Figure 20. Response of circular cavity to traction varying as Ricker wavelets: (a) $\lambda = 200$ and (b) $\lambda = 2000$.

For the mode $\lambda = 2000$, the ratio of dominant dimensionless frequency a_0 to the eigenvalue $\lambda = 2000$ becomes $a_0/\lambda = 0.5$. The $M_H = 32$ singly asymptotic solution for the dynamic stiffness coefficient shows strong oscillation around the exact solution (Figure 18). This leads to the 'fictitious reflections' in the transient response in Figure 20(b). Reasonably accurate response is obtained by using the $M_H = M_L = 5$ doubly asymptotic open boundary.

In a real finite element analysis, the number of modes (eigenvalues) is often not easy to control. An open boundary should perform well for all modes, including those with very high eigenvalues, at the frequency range of interest. The above example demonstrates that a robust open boundary should ideally perform well for the case of semi-infinite layer with a constant depth.

6. CONCLUSIONS

A novel approach for constructing high-order doubly asymptotic open boundaries of arbitrary order has been proposed. The derivation and implementation are presented for the transient analysis of

DOI: 10.1002/nme

scalar waves in a semi-finite layer with a constant depth and a circular cavity in a full-plane. It is found from theoretical formulations and numerical experiments that

1. When a high-order open boundary for the semi-infinite layer with a constant depth is based solely on a high-frequency continued fraction expansion of the dynamic stiffness, i.e. singly asymptotic, it is equivalent to several well-established high-order open boundaries. A singly asymptotic open boundary performs satisfactorily when the dimensionless frequency (ia_0) content of the excitation is mostly higher than the highest modal eigenvalue (λ), but it is unable to model evanescent waves caused by the part of excitation having dimensionless frequency lower than the highest modal eigenvalue. In a time-domain analysis, the error in modeling evanescent waves appears as numerical pollution similar to the 'fictitious reflections' caused by simple boundary conditions.
2. As the modal eigenvalue λ of a circular cavity increases, the dynamic stiffness of the mode tends to that of a mode of a semi-infinite layer. Therefore, a robust open boundary for circular waves should also be able to model evanescent waves.
3. The dynamic stiffness of a doubly asymptotic open boundary converges rapidly to the exact solution in the frequency domain as its order increases. Evanescent waves and late-time (low-frequency) responses are simulated accurately. The doubly asymptotic open boundary shows significant improvement in accuracy in comparison with the singly asymptotic open boundary with the same number of terms.
4. The high-order doubly asymptotic open boundaries are expressed as first-order ordinary differential equations in time. The two time-independent coefficient matrices, the static stiffness and damping matrices, are symmetric and tri-diagonal. Well-established time-stepping schemes in structural dynamics are directly applicable. The amount of computer time and storage are the same as those required by the singly asymptotic open boundary of the same order.

Research on developing a doubly asymptotic open boundary for unbounded domains with arbitrary geometry by extending the work in Reference [40] is in progress.

ACKNOWLEDGEMENTS

Chongmin Song performed some of the research reported herein during his visit to the Dalian University of Technology. The support provided by the Dalian University of Technology and the Natural Science Foundation of China (Grant No. 90510018) through the Hai-Tian scholar scheme is gratefully acknowledged.

REFERENCES

1. Luco JE. Linear soil–structure interaction: a review. In *Earthquake Ground Motion and Its Effects on Structures*, Datta SK (ed.), vol. AMD 53, 1982; 41–57.
2. Kausel E. Local transmitting boundaries. *Journal of Engineering Mechanics* (ASCE) 1988; **114**:1011–1027.
3. Givoli D. Non-reflecting boundary conditions: a review. *Journal of Computational Physics* 1991; **94**:1–29.
4. Tsynkov SV. Numerical solution of problems on unbounded domains: a review. *Applied Numerical Mathematics* 1998; **27**:465–532.
5. Astley RJ. Infinite elements for wave problems: a review of current formulations and an assessment of accuracy. *International Journal for Numerical Methods in Engineering* 2000; **49**:951–976.
6. Givoli D. High-order local non-reflecting boundary conditions: a review. *Wave Motion* 2004; **39**:319–326.
7. Wolf JP. *Dynamic Soil–structure Interaction*. Prentice-Hall: Englewood Cliffs, NJ, 1985.

DOI: 10.1002/nme

8. Wolf JP. *Soil–structure-Interaction Analysis in Time Domain*. Prentice-Hall: Englewood Cliffs, NJ, 1988.
9. Givoli D. *Numerical Methods for Problem in Infinite Domains*. Elsevier: Amsterdam, 1992.
10. Wolf JP, Song Ch. *Finite-element Modelling of Unbounded Media*. Wiley: Chichester, 1996.
11. Hall WS, Oliveto G. *Boundary Element Methods for Soil–structure Interaction*. Kluwer Academic Publishers: Dordrecht, 2003.
12. Beskos DE. Boundary element methods in dynamic analysis. *Applied Mechanics Reviews* (ASME) 1987; **40**:1–23.
13. Kausel E. Thin layer method: formulation in time domain. *International Journal for Numerical Methods in Engineering* 1994; **37**:927–941.
14. Song Ch, Wolf JP. The scaled boundary finite element method—alias consistent infinitesimal finite element cell method—for elastodynamics. *Computer Methods in Applied Mechanics and Engineering* 1997; **147**:329–355.
15. Wolf JP. Consistent lumped-parameter models for unbounded soil: physical representation. *Earthquake Engineering and Structural Dynamics* 1991; **20**:11–32.
16. Paronesso A, Wolf JP. Global lumped-parameter model with physical representation for unbounded medium. *Earthquake Engineering and Structural Dynamics* 1995; **24**:637–654.
17. Alpert B, Greengard L, Hagstrom T. Nonreflecting boundary conditions for the time-dependent wave equation. *Journal of Computational Physics* 2002; **180**:270–296.
18. Ruge P, Trinks C, Witte S. Time-domain analysis of unbounded media using mixed-variable. *Earthquake Engineering and Structural Dynamics* 2001; **30**:899–925.
19. Paronesso A, Wolf JP. Recursive evaluation of interaction forces and property matrices from unit-impulse response functions of unbounded medium based on balancing approximation. *Earthquake Engineering and Structural Dynamics* 1998; **27**:609–618.
20. Lysmer J, Kuhlemeyer RL. Finite dynamic model for infinite media. *Journal of Engineering Mechanics* (ASCE) 1969; **95**:859–877.
21. Smith WD. A nonreflecting plane boundary for wave propagation problems. *Journal of Computational Physics* 1974; **15**:492–503.
22. Engquist B, Majda A. Radiation boundary conditions for acoustic and elastic wave calculations. *Communications on Pure and Applied Mathematics* 1979; **32**:313–357.
23. Liao ZP, Wong HL. A transmitting boundary for the numerical simulation of elastic wave propagation. *Soil Dynamics and Earthquake Engineering* 1984; **3**:174–183.
24. Bayliss A, Gunzburger M, Turkel E. Boundary conditions for the numerical solution of elliptic equations in exterior regions. *SIAM Journal on Applied Mathematics* 1982; **42**:430–451.
25. Higdon RL. Absorbing boundary conditions for difference approximations to the multi-dimensional wave equation. *Mathematics of Computation* 1986; **47**:437–459.
26. Hagstrom T, Hariharan SI. A formulation of asymptotic and exact boundary conditions using local operators. *Applied Numerical Mathematics* 1998; **27**:403–416.
27. Grote MJ, Keller JB. Exact nonreflecting boundary condition for elastic waves. *SIAM Journal on Applied Mathematics* 2000; **60**:803–819.
28. Guddati MN, Tassoulas JL. Continued-fraction absorbing boundary conditions for the wave equation. *Journal of Computational Acoustics* 2000; **8**:139–156.
29. Thompson LL, Huan RN, He DT. Accurate radiation boundary conditions for the two-dimensional wave equation on unbounded domains. *Computer Methods in Applied Mechanics and Engineering* 2001; **191**:311–351.
30. Krenk S. Unified formulation of radiation conditions for the wave equation. *International Journal for Numerical Methods in Engineering* 2002; **53**:275–295.
31. Givoli D, Neta B. High-order non-reflecting boundary scheme for time-dependent waves. *Journal of Computational Physics* 2003; **186**:24–46.
32. Hagstrom T, Warburton T. A new auxiliary variable formulation of high-order local radiation boundary conditions: corner compatibility conditions and extensions to first-order systems. *Wave Motion* 2004; **39**:327–338.
33. Geers TL. Singly and doubly asymptotic computational boundaries. In *Proceedings of the IUTAM Symposium on Computational Methods for Unbounded Domains*, Geers TL (ed.). Kluwer Academic Publishers: Dordrecht, 1998; 135–141.
34. Hagstrom T, Mar-Or A, Givoli D. High-order local absorbing conditions for the wave equation: extensions and improvements. *Journal of Computational Physics* 2008; **227**:3322–3357.
35. Geers TL. Doubly asymptotic approximations for transient motions of submerged structures. *Journal of the Acoustical Society of America* 1978; **63**:1500–1508.
36. Underwood P, Geers TL. Doubly asymptotic, boundary-element analysis of dynamic soil–structure interaction. *International Journal of Solids and Structures* 1981; **17**:687–697.

DOI: 10.1002/nme

37. Geers TL, Zhang P. Doubly asymptotic approximations for submerged structures with internal fluid volumes. *Journal of Applied Mechanics* 1994; **61**:893–906.
38. Geers TL, Lewis BA. Doubly asymptotic approximations for transient elastodynamics. *International Journal of Solids and Structures* 1997; **34**:1293–1305.
39. Geers TL, Toothaker BJ. Third-order doubly asymptotic approximations for computational acoustics. *Journal of Computational Acoustics* 2000; **8**:101–120.
40. Bazyar MH, Song CH. A continued-fraction-based high-order transmitting boundary for wave propagation in unbounded domains of arbitrary geometry. *International Journal for Numerical Methods in Engineering* 2008; **74**:209–237.
41. Givoli D. Recent advances in the DtN FE method. *Archives of Computational Methods in Engineering* 1999; **6**:71–116.
42. Engquist B, Majda A. Absorbing boundary conditions for the numerical simulation of waves. *Mathematics of Computation* 1977; **31**:629–651.
43. Higdon RL. Numerical absorbing boundary conditions for the wave equation. *Mathematics of Computation* 1987; **49**:65–90.
44. Birk C, Ruge P. Representation of radiation damping in a dam–reservoir interaction analysis based on a rational stiffness approximation. *Computers and Structures* 2007; **85**:1152–1163.
45. Harari I, Djellouli R. Analytical study of the effect of wave number on the performance of local absorbing boundary conditions for acoustic scattering. *Applied Numerical Mathematics* 2004; **50**:15–47.

DOI: 10.1002/nme